HHS Public Access

Author manuscript

Acta Biomater. Author manuscript; available in PMC 2017 January 15.

Published in final edited form as:

Acta Biomater. 2016 January 15; 30: 49–61. doi:10.1016/j.actbio.2015.11.029.

Cell Penetrating Peptide-Modified Poly(Lactic-co-Glycolic Acid) Nanoparticles with Enhanced Cell Internalization

Jill M. Steinbach, Ph.D.[1,*], **Young-Eun Seo**[1], and **W. Mark Saltzman**[1]

[1]Department of Biomedical Engineering, Yale University, New Haven, CT, 06520, U.S.A.

Abstract

The surface modification of nanoparticles (NPs) can enhance the intracellular delivery of drugs, proteins, and genetic agents. Here we studied the effect of different surface ligands, including cell penetrating peptides (CPPs), on the cell binding and internalization of poly(lactic-co-glycolic) (PLGA) NPs. Relative to unmodified NPs, we observed that surface-modified NPs greatly enhanced cell internalization. Using one CPP, MPG (unabbreviated notation), that achieved the highest degree of internalization at both low and high surface modification densities, we evaluated the effect of two different NP surface chemistries on cell internalization. After 2 hr, avidin-MPG NPs enhanced cellular internalization by 5 to 26-fold relative to DSPE-MPG NP formulations. Yet, despite a 5-fold increase in MPG density on DSPE- relative to Avidin-NPs, after 24 hr., both formulations resulted in similar internalization levels (48 and 64-fold, respectively). Regardless of surface modification, all NPs were internalized through an energy-dependent, clathrin-mediated process, and became dispersed throughout the cell. Overall both Avidin- and DSPE-CPP modified NPs significantly increased internalization and offer promising delivery options for applications in which internalization presents challenges to efficacious delivery.

Keywords

Nanoparticle; Drug Delivery; Cell Penetrating Peptides; Gene Delivery

INTRODUCTION

Polymer nanoparticles (NPs) are attractive options for the delivery of drugs, proteins, and genetic agents. In particular, polymeric NPs can be especially useful for the delivery of biologics, as they can encapsulate and protect proteins and oligonucleotides (ONs) from degradation, while conferring the delivery advantages of: prolonged stability, controlled

[*]Corresponding author: Tel.: 502-852-5486; Fax: 502-852-5468; jill.steinbach@louisville.edu.
W. Mark Saltzman, Yale University, 55 Prospect Street, Malone 413, New Haven, CT 06511
Jill M. Steinbach, Ph.D., University of Louisville, 505 S. Hancock St., CTRB, Room 623, Louisville, KY 40202
Young Eun-Seo, Yale University, 55 Prospect Street, Malone 401F, New Haven, CT 06511

DISCLOSURES

The authors do not have any conflicts of interest.

release, increased loading, targeting capabilities, and low toxicity in one modality [1-4]. When paired with the delivery of small-interfering RNA (siRNA) or other ONs to promote gene silencing, these carriers offer a viable technology to protect delicate cargo until intracellular localization has occurred, thereby enabling highly specific ONs to bind to or degrade complementary DNA or RNA target sequences.

Of the wide variety of polymeric vehicles utilized to tailor the delivery of biologics [5-9], poly(lactic-co-glycolic acid) (PLGA) NPs have proven markedly successful in combating a number of pathologies, including infectious diseases and cancer, due to their known biocompatibility and efficacy [8, 10-14]. Furthermore, the degradation rate of PLGA – comprised of poly(lactic acid) (PLA) and poly(glycolic acid) (PGA) – can be tailored based on the ratio of these comonomers [15-17]. Whereas higher ratios of hydrophilic PGA increase the degradation rate of PLGA; increased incorporation of the more hydrophobic PLA has the opposite effect [17, 18]. Generally PLGA 50:50, consisting of a 50:50 ratio of PLA to PGA, provides a significantly faster degradation rate than other comonomer ratios, prompting degradation within days to weeks [19, 20]. Additionally, by varying this ratio, PLGA blends may “optimally” tailor the delivery rates of encapsulated molecules. Relative to PLGA, the use of either PGA or PLA alone has been limited by hydrolytic instability (PGA) [21, 22] and slow degradation rate (PLA) [10].

Previous work in our group has demonstrated the successful delivery of siRNA and other ONs from unmodified PLGA (50:50) NPs [3, 4]. We have shown that unmodified siRNA-encapsulated PLGA (50:50) NPs elicit both mRNA knockdown and significant therapeutic effect when delivered intravaginally against HSV-2 infection in a murine model [3, 4]. Similarly, we demonstrated therapeutic efficacy of siRNA (siSurvivin) PLGA (50:50) NPs in an *in vivo* bladder cancer model [23]. Although unmodified NPs successfully delivered siRNA, decreased gene expression *in vitro* and *in vivo*, and provided therapeutic efficacy [3, 4], polymeric delivery vehicles – like other gene delivery platforms – must overcome the challenges associated with intracellular delivery to exert maximum effect [2, 24-27]. Therefore we hypothesized that modifying the NP surface with ligands specific for cell uptake and endosomal escape may enhance cell binding and internalization. To address this hypothesis, we chose to quantify and compare the intracellular delivery of our previously established unmodified PLGA 50:50 NPs with surface-modified PLGA 50:50 NPs, to better understand the differences between, and the fate of NPs during cell association and internalization.

At the cellular level, the primary endocytotic mechanisms of NP internalization include phagocytosis, a process by which specialized cells transport carriers via phagosomes and phagolysosomes for degradation, and pinocytosis, in which the cellular uptake of fluids and molecules occurs within small vesicles. Four types of pinocytosis are currently known, including macropinocytosis, clathrin and caveolin-mediated endocytosis, and clathrin/caveolin independent endocytosis [28, 29]. NPs internalized by the cell via one of these mechanisms may be: sorted into endosomes, and subsequently entrapped and degraded in lysosomal compartments; may be released or escape directly into the cytoplasm; or undergo cellular recycling [28, 29]. For NP-encapsulated agents to exert maximum effect in the cytosol, it is imperative that NP delivery be optimized to increase cell uptake and endosomal

escape [24]. While NPs offer a promising way to deliver agents, NP internalization is impacted by several factors including size, material, surface modification, surface charge, and shape [30-33]. Furthermore, the rate and mechanism of internalization is cell-type dependent and varies based on these factors, making NP design for optimal cellular uptake a challenge [31, 34].

To enhance the internalization of hydrophobic and negatively-charged PLGA NPs, a major focus is on the discovery and incorporation of ligands as surface modifications that improve target cell association and internalization. CPPs, comprised of short, polycationic or amphipathic peptides, have significantly improved the delivery of a variety of molecules, including siRNA, plasmid DNA, antisense ONs, PNA, proteins, and peptides [35-40]. CPPs have been designed to overcome both extracellular and intracellular barriers, by promoting movement of cargo across cell membranes and in some cases enabling the release of molecules trapped inside endosomes into the cytoplasm [41, 42]. Due to the partly hydrophobic and cationic nature of some CPPs, they are able to penetrate the negatively-charged cell membrane at low micromolar concentrations without inflicting membrane damage [43].

Importantly, CPPs can promote the internalization of conjugated cargo such as NPs; however, the role of CPPs in the transport of NPs – which are much larger than single molecules or complexed oligonucleotides – across the cell membrane is not well understood [31, 44]. Internalization of CPPs attached to cargo depends on both the physical properties of the CPP, together with factors including the nature of the cargo and the concentration used [45]. In some cases, the mechanism of uptake for a CPP alone (unconjugated CPP) can be quite different relative to its uptake when attached to cargo such as NPs [46, 47], due to conformational changes in the CPP after conjugation.

Recent work by our group and others has focused on increasing the cellular internalization of drug delivery vehicles, by surface modification with these cell targeting and positively-charged ligands [1, 2, 23, 48-50]. To conjugate CPPs to the surface of our NPs, we combined our siRNA PLGA approach with prior expertise in our lab that established two different surface-modification chemistries – avidin and DSPE-PEG [1, 51]. These surface chemistries had been assessed *in vitro* and *in vivo* with different ligands to provide tumor targeting and mucosal diffusion [1, 52-57]. Based on this previous work, we knew that avidin-modification alone enhances cell uptake and allows conjugation of a variety of peptides [1, 53, 54], and that DSPE-PEG, of different molecular weights, can alter transport and release characteristics (e.g. mucosal) of encapsulant [55]. In this previous work, utilization of PEG chain lengths greater than 2 kDa enabled similar or enhanced diffusion properties when conjugated to the NP surface, with the absolute diffusion coefficient dependent on DSPE-PEG modification density. Therefore for this study, we selected DSPE-PEG(2000) as the surface-modification chemistry to balance diffusive and encapsulant release properties that might be hindered by longer chain lengths in future applications.

In this work we produced NPs that were modified to include surface attachment of chitosan and several different CPPs: penetratin (AP), end-binding protein 1 (EB1), MPG, and MPGΔNLS. Chitosan, a polysaccharide, was included for comparison with CPPs because of

its known benefit in cell/mucoadhesion and tight junction penetration. AP, a 16 amino acid sequence from the third helix of the antennapedia homeodomain, is one of the most studied CPPs with demonstrated success in achieving increased cell penetration [58]. EB1 is a derivative of AP with a triple helix believed to aid in endosomal escape [59]. MPG is a peptide that combines the fusion sequence of HIV (gp41) with the nuclear localization sequence (NLS) of the SV40 antigen. MPGΔNLS contains a single amino acid mutation in the NLS sequence to reduce nuclear localization [41, 60].

In this study we: 1) tested these ligands, known to individually promote cell adhesion, uptake and/or endosomal escape, to determine those that provided the best cell binding and internalization after conjugation to the surface of PLGA NPs, 2) compared two different surface modification chemistries using the CPP that provided the highest cellular internalization, 3) evaluated the effect of surface ligand density on NP uptake, and 4) tracked the endocytotic pathway of CPP-NPs. To our knowledge this is the first study to test these two different surface-modified PLGA NPs with an assortment of ligands, and to demonstrate the predominant mechanism of action of the most readily internalized NP formulation.

MATERIALS AND METHODS

Materials

Poly(lactic co-glycolic acid) with a carboxyl terminus (PLGA, 50:50 monomer ratio and 0.55-0.75 dL/g inherent viscosity) was purchased from LACTEL®. The lipid, 1,2-distearoyl-sn-glycero-3-phosphoethanolamine-N-[carboxy(polyethylene glycol)-2000] (DSPE-PEG), used for one of the surface modifications was purchased from Avanti Polar Lipids. The following peptides were synthesized with an N-terminus cysteine or biotin, followed by a serine-glycine spacer, and were RP-HPLC purified by the W.M. Keck Peptide Synthesis Facility at Yale University (New Haven, CT):

Penetratin (AP): SG-RQIKIWFQNRRMKWKK

End binding protein 1 (EB1): SG-LIRLWSHLIHIWFQNRRLKWKKK

MPG: SG-GALFLGFLGAAGSTMGAWSQPKKKRKV

MPGΔNLS: SG-GALFLGFLGAAGSTMGAWSQPKSKRKV

For uptake inhibition studies, the following chemicals were purchased: Dynasore (Enzo Life Sciences), Chlorpromazine (Sigma), Nystatin (Sigma) and LY294002 (Cell Signaling Technology). To determine intracellular localization, the following primary antibodies were ordered from Cell Signaling Technology and used to stain intracellular proteins: EEA1 (C45B10) rabbit mAb, Rab5 (C8B1) rabbit mAb, Rab7 (D95F2) XP™, clathrin heavy chain (CHC) (D3C6) XP® rabbit mAb, and Rab11 (D4F5) XP® rabbit mAb. LAMP-1, a mouse mAb, was ordered from Santa Cruz Biotechnology. Donkey anti-mouse and anti-rabbit rhodamine-conjugated secondary antibodies were purchased from Invitrogen.

Synthesis of DSPE-PEG and Avidin-Palmitate Conjugates

For CPP modified NPs, 2 different surface modifications were used to modify the NP surface to attach the CPPs: 1) avidin-palmitate to attach biotinylated ligands, or 2) DSPE-PEG conjugated peptides.

Avidin-palmitate was conjugated as previously described [61]. Briefly, 10 mg of avidin was dissolved in 1.2 mL of 2% sodium deoxycholate (NaDC) in phosphate buffered saline (PBS) warmed to 37°C. Palmitic acid-NHS (PA-NHS, Sigma) was dissolved in 2% NaDC at 1 mg/mL and sonicated until well-mixed. Eight hundred microliters of the 1 mg/mL PA-NHS solution was added dropwise to the reaction vial, and reacted overnight at 37°C. The following day, the reaction was dialyzed in 1200 mL of 0.15% NaDC in PBS heated to 37°C with 3500 MWCO dialysis tubing to remove free PA-NHS. The solution was dialyzed overnight at 37°C, and dialysis cassette contents were transferred to a storage vial and stored at 4°C.

DSPE-PEG-peptide conjugates were synthesized as previously described [62]. Briefly, DSPE-PEG(2000)-Maleimide (MW 2941, Avanti Polar Lipids) was conjugated to the N-terminal cysteines of the peptides. The peptides were dissolved in 200 μL DI water for 10 min at room temperature (RT). One hundred microliters of peptide were added to a reaction buffer (Bond-Breaker TCEP-Pierce) containing TCEP to reduce the disulfide bonds. After 1 hr, 3× molar excess of DSPE-PEG-maleimide relative to free peptide in 500 μL reaction buffer was added to the peptide mixture and dissolved with sonication. The reaction was incubated and rotated overnight at RT and was subsequently dialyzed to remove free peptide and DSPE-PEG in PBS. DSPE-PEG-peptide conjugation was verified using matrix assisted laser desorption/ionization (MALDI).

Nanoparticle Synthesis

We synthesized and characterized unmodified and surface-modified PLGA NPs, encapsulating the fluorescent dye Coumarin 6 (C6) for binding and internalization studies, and siRNA to measure bioactivity.

C6 NPs—C6 NPs were synthesized as previously described using an oil-in-water (o/w) single emulsion technique [55]. Briefly, C6 was encapsulated into 100-200 mg poly(lactic co-glycolic acid) carboxyl-terminated polymer (0.55-0.75 dL/g, LACTEL®). PLGA was dissolved overnight in 1 mL methylene chloride (DCM). Similarly, C6 was dissolved in 200 μL methylene chloride (DCM) overnight at a concentration of 15 μg C6 per mg of PLGA. The following day, C6 was added to 100-200 mg PLGA while vortexing. For DSPE-PEG-peptide modified NPs, preconjugated DSPE-PEG-peptides at 0.5, 2, 5, and 10 nmol DSPE/mg PLGA peptide-to-polymer concentrations, were added dropwise to a 5% polyvinyl alcohol (PVA) solution of equal volume and vortexed. For the various DSPE-PEG-peptide ratios added (0.5, 2, 5, and 10 nmol DSPE/mg PLGA), peptide absorbance was measured to determine stock concentrations. The PLGA-C6 solution was then added dropwise to this PVA DSPE-PEG-peptide solution, vortexed, and sonicated. The resulting NPs were hardened during solvent evaporation in 0.3% PVA for 3 hr. After hardening, the NPs were washed and centrifuged at 4°C, 3 times in deionized water (diH_2O) to remove

residual solvent. Non-conjugated DSPE-PEG-peptides and unconjugated peptides were also removed during the wash steps. NPs were frozen, lyophilized, and stored at −20°C until use.

For NPs modified with avidin-palmitate, a similar protocol was followed. Two different NP formulations were synthesized by adding either low (Av L, L = 1 mg/mL) or high (Av H, H = 5 mg/mL) avidin-palmitate to the 5% PVA solution. NPs were collected after the first wash, and incubated for 30 min. with biotinylated ligands at a molar ratio of 3:1 ligand:avidin in PBS. After conjugation, the NPs were washed 2 more times with diH_2O by centrifugation and subsequent washing, were frozen, and lyophilized. All NPs were stored at −20°C after synthesis. Unmodified C6 NPs were prepared similarly, however 5% PVA was added without DSPE-PEG-peptide or avidin-palmitate.

Nanoparticle Characterization—To determine C6 loading, C6 NPs were dissolved in DMSO for 1 hr, and extracted C6 (C6 per mg PLGA) was quantified using a fluorescent plate reader (480/515 nm), and compared to a known standard of C6 in DMSO.

Particle size and morphology were determined using scanning electron microscopy (XL-30 ESEM-FEG scanning electron microscope (SEM) (FEI Company, USA). Dry NPs were mounted on carbon tape and sputter coated with a thin layer of gold (25 nm) under vacuum in an argon atmosphere for 30 s (Dynavac Mini Coater, Dynavac, USA). Average particle diameter and size distribution were determined from SEM images of at least 400 particles per batch using image analysis software (ImageJ, National Institutes of Health). Zeta potential and dynamic light scattering were measured with a Zetasizer Nano ZS (Malvern) in diH_2O to determine particle charge and hydrated diameter. The surface density of DSPE-MPG and Av-MPG on the NPs was quantified using two different methods. In the first, the “background” concentration of avidin on Av-only NPs (from the same batch used to modify with CPPs), was assessed using the Micro BCA protein assay kit (Pierce). Background readings of the Av-only NPs were subtracted from the MicroBCA readings of Av-MPG NP groups to quantify MPG ligand density. To validate the surface density of MPG determined using the MicroBCA assay, we also utilized an indirect method to assess the binding of biotin-FITC to unconjugated sites on Av-MPG NPs (Nanocs, excitation/emission 488/515 nm). Briefly, a 5-fold excess of biotin-FITC to total avidin sites was incubated with Av-MPG or Av-only NPs. By quantifying the total number of biotin-FITC molecules on Av-only NPs and subtracting the number of biotin-FITC molecules present on Av-MPG NPs, we confirmed similar MPG surface densities as those determined using the MicroBCA assay.

Cellular Uptake of Nanoparticles—Flow cytometry (FACS) was used to quantify the total cellular association (binding and internalization) and internalization of NPs. HeLa cells were plated the day prior to NP incubation in 6-well plates at a density of 200,000 cells/well to obtain ~ 40% confluency on the day of treatment. Prior to cell administration, 0.25 mg/mL NPs were suspended in 1× PBS and added to plated cells. This resulted in a final NP treatment concentration of 0.05 mg/mL NPs. Cells were incubated for time points including 2, 4, and 24 hr at 37°C for most experiments. After treatment, cells were washed 5× with PBS++ (containing calcium, magnesium) and harvested using cell dissociation buffer. After cells were suspended, they were transferred to an eppendorf, centrifuged at 400 rcf for 5

min, and the supernatant was removed. Cells were washed in FACS buffer (1% BSA, 0.1% NaN_3 in PBS) and centrifuged again. Half the supernatant was resuspended in FACS buffer and kept on ice (total associated samples) and the other tube was treated with 100 μL trypan blue for 5 min at RT to quench extracellular fluorescence for measurement of internalization. Trypan blue was removed by centrifuging and washing 2× with 1mL FACS buffer. After two washes, the cells were resuspended in FACS buffer, kept on ice, and analyzed on a BD Biosciences FACScan (San Jose, CA).

Confocal Microscopy

HeLa cells were plated in Lab-Tek™ 8-well chambered coverglass at a density of 50,000 cells/well, to obtain 60% cell confluency on the day of treatment. Cells were incubated with various formulations of C6 NPs at a final concentration of 200 μg/mL for times including 2, 4, and 24 hr.

For staining with Texas Red Phalloidin (Invitrogen), the wells were washed 5× with PBS to remove unbound NPs. Cells were fixed with 4% paraformaldehyde for 10 min RT, followed by a 2× PBS wash. Cells were permeabilized with 0.1% Triton X-100 in 1% BSA PBS for 10 min RT, followed by a 2× PBS wash. Cells were incubated with a 1:40 Texas Red Phalloidin in 1% BSA PBS for 20 min RT, and washed twice with PBS. Cell nuclei were stained with Hoechst 33342 (4 μg/mL, Invitrogen) in PBS for 10 min at 37°C, washed with PBS 2×. Cells were mounted in VECTASHIELD® (Vector Laboratories) non-hardening mounting medium at a volume of 0.12 mL/well, and kept at 4°C until imaging.

For live staining with LysoTracker® Red (Invitrogen), cells were treated with NPs as above and washed 5× with PBS after incubation. They were stained with Hoechst for 10 min (4 μg/mL) and washed with 2× PBS++, followed by subsequent staining for 45 min with 200 nM Lysotracker per manufacturers protocol. After rinsing again with PBS++, fresh media was added to the wells for imaging. Live cells were analyzed using a Leica TCS SP5 Confocal Microscope.

Mechanism of Uptake – Inhibitor Studies

To investigate the mechanism of NP uptake, we used a variety of pharmacological inhibitors known to interfere with clathrin, caveolae, and macropinocytotic uptake. Chlorpromazine (CPZ) was chosen to inhibit clathrin-mediated endocytosis, as it specifically exerts its effect on the clathrin-dependent pathway, with no effect on caveolae or other endocytotic mechanisms [63-66]. Nystatin interacts with cholesterol and inhibits caveolae-mediated uptake [44, 66-68]. Dynasore interferes with dynamin and exerts an effect on both clathrin and caveolin-mediated processes [44, 69]. LY294002 inhibits the PI3 kinase enzyme involved in metabolism, which has a role in vesicle formation, and is used as an inhibitor of macropinocytosis [70-73]. For pathway inhibition studies, cells were plated the same as above, however were incubated for one hour in serum free media with 400 μM Dynasore [74], 10 μg/mL Chlorpromazine (CPZ) [63-65], 5 μg/mL Nystatin [63, 67, 68] and 50 μM LY294002 [31, 44], prior to NP treatment. For Dynasore and CPZ, concentrations were optimized to see negligible Transferrin-Alexa Fluor 488 (ThermoFisher, T13342) uptake and for Nystatin, negligible cholera toxin B (CTB-FITC, Sigma C1655) uptake. After 1 hr

preincubation, NPs were added at 0.05 mg/mL to media containing inhibitor. After 4 hr, cells were washed, harvested, and processed for FACS as described above.

Intracellular Localization

Circular glass coverslips (12 mm) were incubated in ethanol for 5-10 min to sterilize. After sterilization, coverslips were placed in 24-well plates, and cells were plated at a density of 75,000 cells/well. The following day cells were treated with 200 μg/mL NPs and incubated for 24 hr. After treatment, cells were washed with PBS++ and fixed with 1% paraformaldehyde in PBS for 10 min, washed again, and permeabilized with 0.3% triton/PBS for 20 min. Cells were blocked against nonspecific binding by adding 5% normal donkey serum diluted in 0.3% Triton, 1% BSA, PBS for 1 hr, and subsequently cells were incubated with 200 μL primary antibody diluted 1:100 in PBS with 0.3% triton, 1% BSA overnight at 4°C. The next day, cells were washed 3× with 1% BSA, PBS and incubated with 200 μL of secondary antibody (donkey anti-mouse and donkey anti-rabbit) at a dilution of 1:1000 in 0.3% triton, 1% BSA PBS for 1.5 hr RT. Cells were washed 3 times with PBS again and coverslips were mounted in ProLong® Gold antifade with DAPI (Invitrogen). Live cells were imaged as above using confocal microscopy.

Statistical Analysis

Experiments were conducted with a minimum sample size of n = 3 for each experiment. Data were analyzed using a two-sided Student's t-test with a p-value of 0.05 or less defined as the threshold for statistical significance.

RESULTS

Nanoparticle Characterization

Previous studies have demonstrated the utility of coupling peptides to NP surfaces via avidin-biotin-ligands (Av-ligand) [61] or DSPE-PEG-peptides [1] (Figure 1). In this study, surface modification of NPs with Av-MPG led to NPs of comparable average size; whereas modification with DSPE-PEG-MPG resulted in seemingly higher values – but with no observed statistical difference (Figure 2A). Analysis of SEM images show average NP diameters of 128 ± 53, 124 ± 54, and 186 ± 72 nm, for unmodified, Av-MPG, and DSPE-MPG NPs respectively. NP surface charge was measured by zeta potential, and DLS was used to measure the hydrodynamic diameter (Figures 2B/C). Average hydrodynamic diameters determined via DLS were roughly equal: 330 ± 63, 389 ± 5, and 325 ± 12 nm for the unmodified, Av-MPG, and DSPE-MPG NPs, respectively. As expected, the diameters measured for hydrated NPs using DLS were higher than diameters determined for unhydrated NPs using SEM – resulting in significant increases of 2.6, 3.1, and 1.7-fold, for unmodified, Av-MPG, and DSPE-MPG NPs respectively.

Zeta potential values were measured for NPs with a range of surface modifications (Figure 2B). Unmodified NPs exhibited a negative charge of −26.5 mV. Addition of avidin to the NPs produced more positive zeta potentials, which correlated with increased avidin density on the NP surface. When CPPs were added to the avidin-modified NPs, the zeta potential was even more positively-charged, again with more positive zeta potentials correlating with

increased ligand density. DSPE-PEG-only addition to the NP surface had only a small effect on zeta potential, when compared to unmodified NPs. Likewise, DSPE-PEG-peptide NPs exhibited negative zeta potentials, near the value of unmodified NPs, regardless of peptide density.

The surface density of peptide resulting from Av-MPG conjugation was less than obtained using DSPE-MPG. Table 1 shows the number of molecules per NP with the respective surface modification. Low (Av-MPG L, L = 1 mg/mL) and high (Av-MPG H, H = 5 mg/mL) Av-MPG modifications resulted in 160 and 940 molecules/NP, whereas DSPE-MPG (0.5, 2, 5, 10 nmol/mg) resulted in 590, 2300, 3500, and 5300 molecules/NP respectively.

Cellular Uptake of Nanoparticles

Cellular Uptake of Avidin-Ligand NPs—Cellular association and internalization were quantitatively assessed using FACS analysis with live HeLa cells incubated with a fixed concentration of NPs (0.05 mg/mL) (Figure 3A). Treatment with unmodified C6, Av, Av-AP, and Av-Chitosan NPs resulted in minimal total association and uptake. All Av-only and Av-ligand NPs exhibited greater total association (binding and internalization) and internalization relative to unmodified NPs. The highest binding and internalization were observed with addition of the CPP EB1 at high surface coverage and with the MPG and MPGΔNLS CPPs at both low (L = 1 mg/mL) and high (H = 5 mg/mL) surface concentrations. These same sets of NPs provided the greatest cell internalization relative to other CPPs at the same modification densities.

We confirmed these results visually, by evaluating NP uptake using confocal microscopy (Figure 3B). After 2 hr incubation with NPs, increases in cell association were observed with both low and high density Av-EB1, Av-MPG, and Av-MPGΔNLS NPs. Furthermore, these surface-modified NPs produced consistently higher levels of intracellular fluorescence than untreated control cells and cells treated with unmodified NPs, after only 2 hr.

Cellular Uptake of Av-MPG vs. DSPE-MPG NPs via Confocal and FACS—HeLa cells were incubated with NPs (0.05 mg/mL) that were surface modified by the addition of DSPE-MPG (0.5, 2, 5, and 10 nmol DSPE/mg PLGA) during synthesis. After 2 hr, a surface concentration-dependent association was seen with the DSPE-MPG formulations, but the proportion of associated NPs that were internalized was small (Figure 4). However, when the incubation time was extended to 24 hr, a strong correlation between MPG surface density and both cell association and uptake was observed by confocal microscopy (Figure 5A) and by FACS (Figure 5B). After 24 hr, surface density-dependent uptake was observed for DSPE-MPG NPs; both association and internalization were higher than with unmodified NPs and DSPE-PEG-only NPs (Figure 5B). Similarly Av-MPG L and Av-MPG H NPs were incubated with HeLa cells for 24 hr to compare uptake, and demonstrated a marked improvement in uptake, relative to Av-only NPs.

Temperature Dependence of Cellular Uptake—To confirm that NP uptake into HeLa cells was active and energy-dependent, NP internalization was measured via FACS at 4 and 37°C (Figure 6). Figures 6A/B show binding and internalization at 4 and 37°C respectively,

for DSPE-MPG NPs, whereas Figures 6C/D show the results of binding/internalization for Av-MPG NPs. At 4°C, a significant decrease in cell internalization was observed for all NP formulations, indicating that cell uptake is primarily an energy-dependent process. At 4 and 37°C all MPG conjugated NPs showed increased total association and increased cell uptake relative to unmodified NPs. For DSPE-MPG NPs, incubation at 4°C decreased cell uptake for the 0.5, 2, 5, and 10 nmol/mg conjugations. Similarly, decreases in binding and internalization resulted for both low and high Av-MPG NPs after incubation at 4°C.

Mechanism of Uptake – Inhibitor Studies

Cellular uptake of unmodified, DSPE-MPG H (10 nmol/mg), and Av-MPG H (5 mg/mL) was measured in the presence of pharmacological inhibitors of endocytosis: CPZ, Nystatin, Dynasore, and LY294002, which are specific for clathrin, caveolin, and macropinocytosis, respectively (Figure 7). Independent of NP modification, or lack thereof, the predominant mechanism of internalization occurred via clathrin-mediated endocytosis. The effects of Nystatin and LY294002 were negligible across formulations.

Intracellular Localization

Intracellular colocalization of Av-MPG and DSPE-MPG C6 NPs (green) with late endosomes and lysosomes (red, Lysotracker) was observed after 24 hr using confocal microscopy (Figure 8). NP trafficking through the lysosomes further confirmed a clathrin-mediated mechanism. To evaluate the subcellular localization of NPs, intracellular colocalization of Av-MPG and DSPE-MPG NPs after 24 hr incubation was quantified using Volocity (Perkin Elmer) to determine the percent of NPs present in various cell compartments (Figure 9). Both DSPE-MPG and Av-MPG NPs were distributed throughout the cell after 24 hr. Approximately 50% of NPs were distributed outside of the stained endosomal pathway compartments, while ~50% were colocalized with endocytotic markers in the various stages of endocytosis spanning: clathrin uptake, early endosomes (EEA1/Rab5), late endosomes (Rab7), recycling compartments (Rab11), and lysosomes (LAMP-1). While many more DSPE-MPG and Av-MPG NPs were internalized after 24 hr relative to unmodified NPs, there was no statistical difference in NP colocalization between the NP groups for each subcellular compartment.

DISCUSSION

Designing NPs that enhance cell binding and direct internalization is critical to achieving efficacy in drug and gene delivery. In previous work we demonstrated that unmodified siRNA PLGA NPs elicit both mRNA knockdown and a therapeutic effect when delivered intravaginally against HSV-2 infection in a murine model [3, 4]. Here, we sought to enhance the intracellular delivery and to obtain a better understanding of the fate of our NPs within the cell. In this work, we modified the surface of PLGA NPs with a variety of ligands, including CPPs, to significantly increase NP internalization. Additionally, we strove to determine the effect surface modification chemistry – using two surface modification strategies [1, 61] – had on the quantity, time frame, and mechanism of NP internalization.

The optimization of NPs for cell internalization is challenging, as cell-NP interactions (including rate, quantity, and mechanism of uptake) are complex – often being size, shape, cell-type, and surface-modification dependent [75]. One way functional groups on the NP surface can influence cell-NP interactions is by altering the NP surface charge. Generally, positively-charged NPs have the greatest cell internalization efficiency, as they interact electrostatically with negatively-charged moieties on the cell surface [33, 76]. For this reason, CPPs have been designed with cationic regions to more strongly interact with the negatively-charged cell membrane, while hydrophobic portions promote internalization through interactions with the lipid membrane. In addition to charge and hydrophobicity, the ligand density on the NP surface can affect internalization and cellular trafficking. Multivalent interactions due to ligand-NP conjugation can dramatically increase the avidity of NPs for cell surface receptors, and have correspondingly increased NP transport into cells [77, 78].

We initially evaluated Av-modified NPs, conjugated with biotinylated ligands at two different surface densities (Figure 3). Of the variety of ligand-conjugated NPs screened, Av-EB1, Av-MPG, and Av-MPGΔNLS NPs resulted in maximum binding and uptake relative to unmodified and Av-only NP controls. Relative to previously studied CPP-modified polymeric NPs whose uptake improved by only 1.5 to 10-fold [1, 79-83], Av-MPG L and H NPs demonstrated the greatest cell internalization, independent of surface ligand density – resulting in the highest increase in internalization relative to unmodified polymer NPs (48 and 64-fold, respectively). Therefore, we chose to focus our subsequent studies evaluating MPG as a model peptide.

By conjugating MPG to our NPs using two different surface modification strategies (Av and DSPE), we sought to examine the influence of surface modification chemistry on cell uptake. While Av-MPG NPs entered the cell quickly (within 2 hr) (Figure 3), DSPE-MPG NPs showed less rapid uptake after 2 hr (Figure 4). However, after 24 hr, both Av-MPG and DSPE-MPG NPs increased cell internalization by similar amounts and by as much as 70-fold relative to unmodified NPs (Figure 5). Therefore, we hypothesize that the more positive zeta potential of Av-modified NPs enhances NP binding to the cell surface through electrostatic interactions, thereby facilitating more rapid uptake of Av-MPG NPs relative to the more negatively-charged DSPE-MPG NPs (Figure 2C). However, after a longer time (24 hr), the DSPE-MPG NPs attain similar levels of internalization as Av-MPG NPs, while displaying more distributed and less punctate binding (Figures 3 and 5). This trend is in agreement with other studies in which positively-charged surface-modifications to PLGA NPs exhibited higher uptake than negatively-charged NPs [33]. However, here we demonstrate a dramatic increase in uptake of CPP-modified NPs relative to unmodified, Av-only, and DSPE-PEG-only NPs [54, 84].

In addition to NP surface charge, we also observed a correlation between cell uptake and ligand density for both Av and DSPE-NPs (Figure 5). Increases in the density of MPG on DSPE-NPs and Av-NPs correlated with increases in both binding and internalization after 24 hr. This is in agreement with a study demonstrating that increasing overall ligand density on the NP surface resulted in increased internalization up to a saturation level [85]. Interestingly however, Av-NPs demonstrated faster and more greatly enhanced cellular

uptake relative to DSPE-NPs despite lower surface ligand density. Av-MPG NPs with ~900 ligands on the surface attained similar uptake as DSPE-MPG NPs with 5× as much ligand. We attribute the overall positive charge of the Av-MPG NPs to this significant enhancement in binding and internalization (despite lower surface MPG density), especially after shorter time periods of exposure.

Although Av or DSPE-NP surface modifications seemed to affect the quantity and rate of NP uptake, CPPs have a distinct mechanism of uptake when delivered alone or complexed to smaller cargo (such as oligonucleotides) [41, 43, 60, 78, 86]. In fact, the established mechanism of internalization for MPG electrostatically complexed with siRNA is direct membrane translocation [43, 87]. Uniquely, this internalization mechanism differs from the proposed endocytotic uptake mechanisms of other CPPs, such as Tat and R9, that enter via clathrin or caveolae-mediated endocytosis [43, 59, 60, 78, 88, 89]. Indeed, we also expected it likely that the cellular uptake mechanism of a CPP would change when conjugated to larger carriers such as NPs. To better understand the internalization mechanism of MPG-modified NPs we explored how they were internalized *in vitro*.

In the presence of different endocytotic inhibitors specific for clathrin, caveolin, and macropinocytosis-mediated uptake, we established that unmodified, Av-MPG, and DSPE-MPG NPs primarily enter the cell in an active, temperature and energy-dependent manner (Figure 6). Furthermore, regardless of surface modification chemistry (Av or DSPE NPs) or lack thereof (unmodified NPs), an inhibitor dose-dependent effect was noted after incubation with CPZ, indicating that NPs are internalized via clathrin-mediated endocytosis (Figure 7). Our finding that Nystatin had negligible effect across unmodified and surface-modified formulations is in agreement with previous studies in that typically, caveolae do not permit internalization of NPs greater than 50-100 nm [31, 44]. Similarly LY294002 exerted negligible effect, exempting macropinocytosis as a primary mechanism of cell uptake.

The above results that exclude caveolae-mediated transport of these NPs into the cell, highlight the role of NP size on internalization pathway, in addition to surface charge and ligand density. While we observed differences between the average unhydrated sizes of unmodified (128 ± 53 nm), Av-MPG (124 ± 54 nm), and DSPE-MPG NPs (186 ± 72 nm) – these differences were not statistically significant. However, when hydrated NPs were measured with DLS, they had corresponding size increases of 2.6, 3.1, and 1.7-fold, relative to their unhydrated sizes. We attribute these notable increases to PLGA and DSPE-PEG absorption and swelling after immersion in aqueous solution [16, 90-94]. Based on the known swelling properties of PLGA and PEG polymers, we expected that DSPE-PEG PLGA NPs would swell more than other formulations; however DSPE-PEG NPs had the smallest increase in hydrodynamic diameter. Instead, we observed the largest increase in hydrated NP size with Av-MPG NPs, resulting in a 3-fold increase in diameter, relative to unmodified (2.6) and DSPE-PEG (1.7) NPs.

One factor contributing to this observed size increase, is the propensity of Av-MPG NPs to aggregate in solution (unpublished observations during formulation). In fact, this is a common phenomenon impacting NP delivery when hydrophobic or surface-charged NPs are

in an aqueous environment [95-97]. In particular for surface-charged NPs, aggregation can occur in more complex aqueous environments that contain serum or other proteins that may bind to and destabilize the NPs [98-100]. While NP aggregation may be difficult to discern using SEM to characterize unhydrated NPs, it is more readily observed with hydrated NPs. Using DLS measurements to assess hydrated NPs, we initially expected that charge-based interactions seen in Av-only or Av-MPG formulations may enable NPs to disperse in non-serum conditions. Instead we observed some level of aggregation even when conducted in DI water. According to classical Derjaguin-Landau-Verwey-Overbeak (DLVO) theory, within a stable zeta potential range of −30 to 30mV, increasing the surface charge or absolute value of zeta potential typically suppresses aggregation, thereby decreasing the NP hydrodynamic size [99, 101]. In fact, charging NPs has been used as a strategy to reduce aggregation [102, 103]. However, expanded theories and experimental validation have suggested that surface-modification of NPs with cationic molecules can induce aggregation that may be further dependent on size, sterics, (bio)macromolecule modification, surface properties, hydrogen bonding, “back binding”, and other equivalent forces acting in parallel to van der Waal and electrical double layer (EDL) forces [100, 101, 104].

Based on the DLS measurements of hydrated Av-only or Av-MPG formulations, and other studies that have demonstrated aggregation with cationic surface modifications in DI water, we believe that a combination of surface charge, surface chemistry, biomacromolecule (avidin-biotin-MPG) modification, and hydrophobic sections of the conjugated peptide may contribute to particle aggregation. Conversely, low DSPE-PEG NPs exhibited larger diameters relative to high DSPE-PEG NPs, indicating potential aggregative effects attributed to the unmodified hydrophobic regions of PLGA NPs.

While there is not a distinct trend noted between hydrated unmodified and surface-modified NP groups, for both low and high DSPE-PEG NPs, we acknowledge that both size and surface charge likely contribute to the observed decrease and less rapid internalization of NPs, despite the increased density of MPG peptide. However, while broad size differences (e.g. sub-100nm vs. 200nm) are known to have an impact on cellular internalization, the size differences observed here are not significant enough to alter the mechanism of internalization. Instead we propose that size contributes to internalization kinetics, and are also strongly influenced by surface charge and ligand density. While we believe that the complex interactions of surface charge, ligand density, and size are contributors to the described trends in NP uptake, here charge-based effects seem to play a dominant role in the significant increase in internalization seen with Av-MPG NPs after only 2 hr.

Finally, it is well known that cargo transported via clathrin-mediated endocytosis can become trapped in lysosomes and degraded. As observed with confocal microscopy (Figure 8), NP trafficking through the endo-lysosomes was observed, leading to partial NP entrapment in these organelles after 24 hr. However, both DSPE-MPG and Av-MPG NPs were distributed throughout the cell after 24 hr (Figure 9). While approximately half the NPs colocalized with endocytotic markers in the various stages of endocytosis spanning clathrin uptake, early endosome transport, to eventually late endosomes and lysosome localization; a substantial fraction of NPs (~50%) either escape from endosomes; enter by some other process; or are located extracellularly. Interestingly, and unexpected to us, while many more

DSPE-MPG and Av-MPG NPs were internalized after 24 hr relative to unmodified NPs, there were similar proportions of NPs in each subcellular compartment.

Although many more DSPE-MPG and Av-MPG NPs were internalized relative to unmodified NPs, the similar pathway taken by all NPs suggests that combined factors play a role in determining internalization, and that surface modification alone may not affect NP trajectory as we anticipated. To truly alter internalization pathway, future considerations may include designing MPG-NPs small enough to utilize the translocating capabilities of MPG or to enter for instance, a caveolae-mediated pathway, to favor NP processing along non-acidic, nondegradative pathways. Broader changes in NP size and shape are likely necessary to mediate the uptake pathway and to increase opportunities to escape endosomes altogether, thereby enhancing transfection efficacy. In future work it would be of interest to consider the combined effects of ligand density and surface charge and a more intricate evaluation of NP size (via different formulations) in regulating cell internalization.

Our studies here demonstrate that modifying PLGA NPs with CPPs provides striking advantages – of almost two orders of magnitude – in cell binding and uptake, relative to unmodified PLGA NPs. Importantly, in our study, MPG, MPGΔNLS, and EB1 all conferred a significant advantage in binding and uptake, as quantitatively measured by FACS and qualitatively visualized with confocal microscopy. Similar amounts of uptake were achieved with DSPE-MPG H NPs relative to Av-MPG NPs, with Av-MPG NPs (L and H) more rapidly internalized. Additionally, Av-MPG NPs were more efficiently internalized despite lesser amounts of MPG on the surface. While surface modification strategy (Av or DSPE) did not alter the internalization pathway, the enhancement in internalization and intracellular localization achieved using MPG-modified NPs provides a promising baseline for delivery applications in which enhanced cell internalization is difficult to achieve with unmodified carriers.

CONCLUSIONS

PLGA NPs are promising delivery vehicles for the intracellular delivery of drugs, proteins, and genetic agents. We observed that surface-modified NPs experience dramatically increased cell internalization over the course of 24 hr, relative to unmodified NPs. Surface-modification chemistry makes a difference in rapidity of initial uptake: Av-MPG NPs were taken into the cell rapidly within 2 hr; whereas DSPE-MPG NPs were less rapidly internalized. However, after 24 hr, both surface-modified NP formulations resulted in similar levels of cell uptake. Furthermore, despite a 5-fold lower Av-MPG density relative to MPG on DSPE-NPs, Av-MPG NPs achieved only slightly higher uptake after 24 hr. Regardless of surface modification, both formulations were internalized predominantly through an energy-dependent, clathrin-mediated process, and similarly distributed throughout the cell – with approximately 50% of NPs ending up outside of the endosomal pathway or bound to the cell surface. Overall, the dramatically increased internalization offers promising options for any application in which binding and internalization present challenges to efficacious drug or gene delivery.

Supplementary Material

Refer to Web version on PubMed Central for supplementary material.

ACKNOWLEDGEMENTS

We acknowledge and thank our funding sources: NIH NIAID Postdoctoral Fellowship (F32AI093056) and the Yale Proteomics and Genomics Training Fellowship (NIH T32-HG003198) (JMS) & NIH R01 EB000487 (WMS).

REFERENCES

[1]. Cheng CJ, Saltzman WM. Enhanced siRNA delivery into cells by exploiting the synergy between targeting ligands and cell-penetrating peptides. Biomaterials. 2011; 32:6194–203. [PubMed: 21664689]

[2]. Gao W, Xiao Z, Radovic-Moreno A, Shi J, Langer R, Farokhzad OC. Progress in siRNA delivery using multifunctional nanoparticles. Methods in molecular biology. 2010; 629:53–67. [PubMed: 20387142]

[3]. Steinbach JM, Weller CE, Booth CJ, Saltzman WM. Polymer nanoparticles encapsulating siRNA for treatment of HSV-2 genital infection. Journal of controlled release: official journal of the Controlled Release Society. 2012; 162:102–10. [PubMed: 22705461]

[4]. Woodrow KA, Cu Y, Booth CJ, Saucier-Sawyer JK, Wood MJ, Saltzman WM. Intravaginal gene silencing using biodegradable polymer nanoparticles densely loaded with small-interfering RNA. Nature materials. 2009; 8:526–33. [PubMed: 19404239]

[5]. Kobsa S, Saltzman WM. Bioengineering approaches to controlled protein delivery. Pediatric research. 2008; 63:513–9. [PubMed: 18427296]

[6]. Pagels RF, Prud'homme RK. Polymeric nanoparticles and microparticles for the delivery of peptides, biologics, and soluble therapeutics. Journal of controlled release: official journal of the Controlled Release Society. 2015

[7]. Skalko-Basnet N. Biologics: the role of delivery systems in improved therapy. Biologics: targets & therapy. 2014; 8:107–14. [PubMed: 24672225]

[8]. Steinbach JM. Protein and oligonucleotide delivery systems for vaginal microbicides against viral STIs. Cellular and molecular life sciences: CMLS. 2015; 72:469–503. [PubMed: 25323132]

[9]. Singh, M.; Salnikova, M. Novel Approaches and Strategies for Biologics, Vaccines and Cancer Therapies. Academic Press; 2014.

[10]. Danhier F, Ansorena E, Silva JM, Coco R, Le Breton A, Preat V. PLGA-based nanoparticles: an overview of biomedical applications. Journal of controlled release: official journal of the Controlled Release Society. 2012; 161:505–22. [PubMed: 22353619]

[11]. Dinarvand R, Sepehri N, Manoochehri S, Rouhani H, Atyabi F. Polylactide-co-glycolide nanoparticles for controlled delivery of anticancer agents. International journal of nanomedicine. 2011; 6:877–95. [PubMed: 21720501]

[12]. Cheng CJ, Saltzman WM. Nanomedicine: Downsizing tumour therapeutics. Nature nanotechnology. 2012; 7:346–7.

[13]. Cheng CJ, Tietjen GT, Saucier-Sawyer JK, Saltzman WM. A holistic approach to targeting disease with polymeric nanoparticles. Nature reviews Drug discovery. 2015; 14:239–47. [PubMed: 25598505]

[14]. Bala I, Hariharan S, Kumar MNVR. PLGA nanoparticles in drug delivery: The state of the art. Crit Rev Ther Drug. 2004; 21:387–422.

[15]. Brannon-Peppas L. Recent advances on the use of biodegradable microparticles and nanoparticles in controlled drug delivery. International journal of pharmaceutics. 1995; 116:1–9.

[16]. Makadia HK, Siegel SJ. Poly Lactic-co-Glycolic Acid (PLGA) as Biodegradable Controlled Drug Delivery Carrier. Polymers. 2011; 3:1377–97. [PubMed: 22577513]

[17]. Shive MS, Anderson JM. Biodegradation and biocompatibility of PLA and PLGA microspheres. Advanced drug delivery reviews. 1997; 28:5–24. [PubMed: 10837562]

[18]. Saltzman, WM. Drug Delivery. Oxford; New York: 2001.

[19]. Schliecker G, Schmidt C, Fuchs S, Kissel T. Characterization of a homologous series of D, L-lactic acid oligomers; a mechanistic study on the degradation kinetics in vitro. Biomaterials. 2003; 24:3835–44. [PubMed: 12818556]

[20]. Park TG. Degradation of Poly(D,L-Lactic Acid) Microspheres - Effect of Molecular-Weight. Journal of Controlled Release. 1994; 30:161–73.

[21]. Gilding DK, Reed AM. Biodegradable polymers for use in surgery - polyglycolic/poly (lactic acid) homo- and copolymers: 1. Polymer. 1979; 20:1459–64.

[22]. Degradable Polymers: Principles and Applications. 2 ed. Springer Science and Business Media; 2002.

[23]. Martin DT, Steinbach JM, Liu J, Shimizu S, Kaimakliotis HZ, Wheeler MA, et al. Surface-modified nanoparticles enhance transurothelial penetration and delivery of survivin siRNA in treating bladder cancer. Molecular cancer therapeutics. 2014; 13:71–81. [PubMed: 24222663]

[24]. Torchilin VP. Cell penetrating peptide-modified pharmaceutical nanocarriers for intracellular drug and gene delivery. Biopolymers. 2008; 90:604–10. [PubMed: 18381624]

[25]. Williford JM, Wu J, Ren Y, Archang MM, Leong KW, Mao HQ. Recent advances in nanoparticle-mediated siRNA delivery. Annual review of biomedical engineering. 2014; 16:347–70.

[26]. Gavrilov K, Saltzman WM. Therapeutic siRNA: principles, challenges, and strategies. The Yale journal of biology and medicine. 2012; 85:187–200. [PubMed: 22737048]

[27]. Kanasty R, Dorkin JR, Vegas A, Anderson D. Delivery materials for siRNA therapeutics. Nature materials. 2013; 12:967–77. [PubMed: 24150415]

[28]. Hillaireau H, Couvreur P. Nanocarriers' entry into the cell: relevance to drug delivery. Cellular and molecular life sciences: CMLS. 2009; 66:2873–96. [PubMed: 19499185]

[29]. Khalil IA, Kogure K, Akita H, Harashima H. Uptake pathways and subsequent intracellular trafficking in nonviral gene delivery. Pharmacol Rev. 2006; 58:32–45. [PubMed: 16507881]

[30]. Hocherl A, Dass M, Landfester K, Mailander V, Musyanovych A. Competitive cellular uptake of nanoparticles made from polystyrene, poly(methyl methacrylate), and polylactide. Macromol Biosci. 2012; 12:454–64. [PubMed: 22362704]

[31]. Iversen T, Skotland T, Sandvig K. Endocytosis and intracellular transport of nanoparticles: Present knowledge and need for future studies. Nano Today. 2011; 6:176–85.

[32]. Vacha R, Martinez-Veracoechea FJ, Frenkel D. Receptor-mediated endocytosis of nanoparticles of various shapes. Nano Lett. 2011; 11:5391–5. [PubMed: 22047641]

[33]. Harush-Frenkel O, Rozentur E, Benita S, Altschuler Y. Surface charge of nanoparticles determines their endocytic and transcytotic pathway in polarized MDCK cells. Biomacromolecules. 2008; 9:435–43. [PubMed: 18189360]

[34]. dos Santos T, Varela J, Lynch I, Salvati A, Dawson KA. Quantitative assessment of the comparative nanoparticle-uptake efficiency of a range of cell lines. Small. 2011; 7:3341–9. [PubMed: 22009913]

[35]. Mussbach F, Franke M, Zoch A, Schaefer B, Reissmann S. Transduction of peptides and proteins into live cells by cell penetrating peptides. J Cell Biochem. 2011; 112:3824–33. [PubMed: 21826709]

[36]. Meade BR, Dowdy SF. Exogenous siRNA delivery using peptide transduction domains/cell penetrating peptides. Advanced drug delivery reviews. 2007; 59:134–40. [PubMed: 17451840]

[37]. Meade BR, Dowdy SF. Enhancing the cellular uptake of siRNA duplexes following noncovalent packaging with protein transduction domain peptides. Advanced drug delivery reviews. 2008; 60:530–6. [PubMed: 18155315]

[38]. Koren E, Torchilin VP. Cell-penetrating peptides: breaking through to the other side. Trends Mol Med. 2012; 18:385–93. [PubMed: 22682515]

[39]. Lehto T, Kurrikoff K, Langel U. Cell-penetrating peptides for the delivery of nucleic acids. Expert Opin Drug Deliv. 2012; 9:823–36. [PubMed: 22594635]

[40]. Margus H, Padari K, Pooga M. Cell-penetrating peptides as versatile vehicles for oligonucleotide delivery. Mol Ther. 2012; 20:525–33. [PubMed: 22233581]

[41]. Morris MC, Deshayes S, Heitz F, Divita G. Cell-penetrating peptides: from molecular mechanisms to therapeutics. Biol Cell. 2008; 100:201–17. [PubMed: 18341479]

[42]. Erazo-Oliveras A, Muthukrishnan N, Baker R, Wang T, Pellois JP. Improving the Endosomal Escape of Cell-Penetrating Peptides and Their Cargos: Strategies and Challenges. Pharmaceuticals. 2012; 5:1177–209. [PubMed: 24223492]

[43]. Madani F, Lindberg S, Langel U, Futaki S, Graslund A. Mechanisms of cellular uptake of cell-penetrating peptides. J Biophys. 2011; 2011:414729. [PubMed: 21687343]

[44]. Zaki NM, Tirelli N. Gateways for the intracellular access of nanocarriers: a review of receptor-mediated endocytosis mechanisms and of strategies in receptor targeting. Expert Opin Drug Deliv. 2010; 7:895–913. [PubMed: 20629604]

[45]. Rydstrom A, Deshayes S, Konate K, Crombez L, Padari K, Boukhaddaoui H, et al. Direct translocation as major cellular uptake for CADY self-assembling peptide-based nanoparticles. PLoS One. 2011; 6:e25924. [PubMed: 21998722]

[46]. Wang J, Lu Z, Wientjes MG, Au JL. Delivery of siRNA therapeutics: barriers and carriers. AAPS J. 2010; 12:492–503. [PubMed: 20544328]

[47]. Chiu YL, Ali A, Chu CY, Cao H, Rana TM. Visualizing a correlation between siRNA localization, cellular uptake, and RNAi in living cells. Chem Biol. 2004; 11:1165–75. [PubMed: 15324818]

[48]. Katas H, Chen S, Osamuyimen AA, Cevher E, Oya Alpar H. Effect of preparative variables on small interfering RNA loaded Poly(D,L-lactide-co-glycolide)-chitosan submicron particles prepared by emulsification diffusion method. J Microencapsul. 2008; 25:541–8. [PubMed: 18465303]

[49]. Nafee N, Taetz S, Schneider M, Schaefer UF, Lehr CM. Chitosan-coated PLGA nanoparticles for DNA/RNA delivery: effect of the formulation parameters on complexation and transfection of antisense oligonucleotides. Nanomedicine. 2007; 3:173–83. [PubMed: 17692575]

[50]. Zhou J, Patel TR, Fu M, Bertram JP, Saltzman WM. Octa-functional PLGA nanoparticles for targeted and efficient siRNA delivery to tumors. Biomaterials. 2012; 33:583–91. [PubMed: 22014944]

[51]. Fahmy TM, Samstein RM, Harness CC, Saltzman WM. Surface modification of biodegradable polyesters with fatty acid conjugates for improved drug targeting. Biomaterials. 2005; 26:5727–36. [PubMed: 15878378]

[52]. Cheng CJ, Bahal R, Babar IA, Pincus Z, Barrera F, Liu C, et al. MicroRNA silencing for cancer therapy targeted to the tumour microenvironment. Nature. 2015; 518:107–10. [PubMed: 25409146]

[53]. Cu Y, Booth CJ, Saltzman WM. In vivo distribution of surface-modified PLGA nanoparticles following intravaginal delivery. Journal of controlled release: official journal of the Controlled Release Society. 156:258–64. [PubMed: 21763739]

[54]. Cu Y, LeMoellic C, Caplan MJ, Saltzman WM. Ligand-modified gene carriers increased uptake in target cells but reduced DNA release and transfection efficiency. Nanomedicine. 2010; 6:334–43. [PubMed: 19800989]

[55]. Cu Y, Saltzman WM. Controlled surface modification with poly(ethylene)glycol enhances diffusion of PLGA nanoparticles in human cervical mucus. Mol Pharm. 2009; 6:173–81. [PubMed: 19053536]

[56]. Park J, Fong PM, Lu J, Russell KS, Booth CJ, Saltzman WM, et al. PEGylated PLGA nanoparticles for the improved delivery of doxorubicin. Nanomedicine: nanotechnology, biology, and medicine. 2009; 5:410–8.

[57]. Park J, Mattessich T, Jay SM, Agawu A, Saltzman WM, Fahmy TM. Enhancement of surface ligand display on PLGA nanoparticles with amphiphilic ligand conjugates. Journal of controlled release: official journal of the Controlled Release Society. 2011; 156:109–15. [PubMed: 21723893]

[58]. Console S, Marty C, Garcia-Echeverria C, Schwendener R, Ballmer-Hofer K. Antennapedia and HIV transactivator of transcription (TAT) “protein transduction domains” promote endocytosis of high molecular weight cargo upon binding to cell surface glycosaminoglycans. The Journal of biological chemistry. 2003; 278:35109–14. [PubMed: 12837762]

[59]. Lundberg P, El-Andaloussi S, Sutlu T, Johansson H, Langel U. Delivery of short interfering RNA using endosomolytic cell-penetrating peptides. FASEB J. 2007; 21:2664–71. [PubMed: 17463227]

[60]. Simeoni F, Morris MC, Heitz F, Divita G. Insight into the mechanism of the peptide-based gene delivery system MPG: implications for delivery of siRNA into mammalian cells. Nucleic Acids Res. 2003; 31:2717–24. [PubMed: 12771197]

[61]. Fahmy TM, Samstein RM, Harness CC, Mark Saltzman W. Surface modification of biodegradable polyesters with fatty acid conjugates for improved drug targeting. Biomaterials. 2005; 26:5727–36. [PubMed: 15878378]

[62]. Cheng CJ, Saltzman WM. Enhanced siRNA delivery into cells by exploiting the synergy between targeting ligands and cell-penetrating peptides. Biomaterials. 32:6194–203. [PubMed: 21664689]

[63]. Benfer M, Kissel T. Cellular uptake mechanism and knockdown activity of siRNA-loaded biodegradable DEAPA-PVA-g-PLGA nanoparticles. Eur J Pharm Biopharm. 2012; 80:247–56. [PubMed: 22085653]

[64]. dos Santos T, Varela J, Lynch I, Salvati A, Dawson KA. Effects of transport inhibitors on the cellular uptake of carboxylated polystyrene nanoparticles in different cell lines. PLoS One. 2011; 6:e24438. [PubMed: 21949717]

[65]. Gotte M, Sofeu Feugaing DD, Kresse H. Biglycan is internalized via a chlorpromazine-sensitive route. Cell Mol Biol Lett. 2004; 9:475–81. [PubMed: 15332124]

[66]. Ivanov, AI. Pharmacological Inhibition of Endocytic Pathways: Is It Specific Enough to Be Useful. In: Ivanov, AI., editor. Methods in molecular biology. Humana Press; NJ: 2008.

[67]. Chen Y, Wang S, Lu X, Zhang H, Fu Y, Luo Y. Cholesterol sequestration by nystatin enhances the uptake and activity of endostatin in endothelium via regulating distinct endocytic pathways. Blood. 2011; 117:6392–403. [PubMed: 21482707]

[68]. Qaddoumi MG, Gukasyan HJ, Davda J, Labhasetwar V, Kim KJ, Lee VH. Clathrin and caveolin-1 expression in primary pigmented rabbit conjunctival epithelial cells: role in PLGA nanoparticle endocytosis. Mol Vis. 2003; 9:559–68. [PubMed: 14566223]

[69]. Gratton SE, Ropp PA, Pohlhaus PD, Luft JC, Madden VJ, Napier ME, et al. The effect of particle design on cellular internalization pathways. Proc Natl Acad Sci U S A. 2008; 105:11613–8. [PubMed: 18697944]

[70]. Araki N, Hatae T, Furukawa A, Swanson JA. Phosphoinositide-3-kinase-independent contractile activities associated with Fc gamma-receptor-mediated phagocytosis and macropinocytosis in macrophages. J Cell Sci. 2003; 116:247–57. [PubMed: 12482911]

[71]. Araki N, Johnson MT, Swanson JA. A role for phosphoinositide 3-kinase in the completion of macropinocytosis and phagocytosis by macrophages. J Cell Biol. 1996; 135:1249–60. [PubMed: 8947549]

[72]. Araki N, Johnson MT, Swanson JA. A role for PI 3-kinase in the closure of macropinosomes and phagosomes in macrophages. Mol Biol Cell. 1996; 7:2627.

[73]. Kruth HS, Jones NL, Huang W, Zhao B, Ishii I, Chang J, et al. Macropinocytosis is the endocytic pathway that mediates macrophage foam cell formation with native low density lipoprotein. J Biol Chem. 2005; 280:2352–60. [PubMed: 15533943]

[74]. Schmidt MR, Maritzen T, Kukhtina V, Higman VA, Doglio L, Barak NN, et al. Regulation of endosomal membrane traffic by a Gadkin/AP-1/kinesin KIF5 complex. Proc Natl Acad Sci U S A. 2009; 106:15344–9. [PubMed: 19706427]

[75]. Harush-Frenkel O, Debotton N, Benita S, Altschuler Y. Targeting of nanoparticles to the clathrin-mediated endocytic pathway. Biochemical and biophysical research communications. 2007; 353:26–32. [PubMed: 17184736]

[76]. Verma A, Stellacci F. Effect of surface properties on nanoparticle-cell interactions. Small. 2010; 6:12–21. [PubMed: 19844908]

[77]. Tassa C, Duffner JL, Lewis TA, Weissleder R, Schreiber SL, Koehler AN, et al. Binding affinity and kinetic analysis of targeted small molecule-modified nanoparticles. Bioconjugate chemistry. 2010; 21:14–9. [PubMed: 20028085]

[78]. Kawamura KS, Sung M, Bolewska-Pedyczak E, Gariepy J. Probing the impact of valency on the routing of arginine-rich peptides into eukaryotic cells. Biochemistry. 2006; 45:1116–27. [PubMed: 16430208]

[79]. Xia H, Gao X, Gu G, Liu Z, Hu Q, Tu Y, et al. Penetratin-functionalized PEG-PLA nanoparticles for brain drug delivery. International journal of pharmaceutics. 2012; 436:840–50. [PubMed: 22841849]

[80]. Wang H, Zhao Y, Wang H, Gong J, He H, Shin MC, et al. Low-molecular-weight protamine-modified PLGA nanoparticles for overcoming drug-resistant breast cancer. Journal of controlled release: official journal of the Controlled Release Society. 2014; 192:47–56. [PubMed: 25003794]

[81]. Liu X, Liu C, Zhang W, Xie C, Wei G, Lu W. Oligoarginine-modified biodegradable nanoparticles improve the intestinal absorption of insulin. International journal of pharmaceutics. 2013; 448:159–67. [PubMed: 23538098]

[82]. Chen J, Li S, Shen Q. Folic acid and cell-penetrating peptide conjugated PLGA-PEG bifunctional nanoparticles for vincristine sulfate delivery. European journal of pharmaceutical sciences: official journal of the European Federation for Pharmaceutical Sciences. 2012; 47:430–43. [PubMed: 22796217]

[83]. Fields RJ, Cheng CJ, Quijano E, Weller C, Kristofik N, Duong N, et al. Surface modified poly(beta amino ester)-containing nanoparticles for plasmid DNA delivery. Journal of controlled release: official journal of the Controlled Release Society. 2012; 164:41–8. [PubMed: 23041278]

[84]. Verma A, Uzun O, Hu Y, Han HS, Watson N, Chen S, et al. Surface-structure-regulated cell-membrane penetration by monolayer-protected nanoparticles. Nature materials. 2008; 7:588–95. [PubMed: 18500347]

[85]. Moradi E, Driton V, Garnett M, Falcone F, Stolnik S. Ligand density and clustering effects on endocytosis of folate modified nanoparticles. RSC Advances. 2012; 2:3025–33.

[86]. Mishra R, Su W, Pohmann R, Pfeuffer J, Sauer MG, Ugurbil K, et al. Cell-penetrating peptides and peptide nucleic acid-coupled MRI contrast agents: evaluation of cellular delivery and target binding. Bioconjugate chemistry. 2009; 20:1860–8. [PubMed: 19788302]

[87]. Deshayes S, Morris MC, Divita G, Heitz F. Interactions of amphipathic CPPs with model membranes. Biochimica et biophysica acta. 2006; 1758:328–35. [PubMed: 16277976]

[88]. Endoh T, Ohtsuki T. Cellular siRNA delivery using cell-penetrating peptides modified for endosomal escape. Advanced drug delivery reviews. 2009; 61:704–9. [PubMed: 19383521]

[89]. Duchardt F, Fotin-Mleczek M, Schwarz H, Fischer R, Brock R. A comprehensive model for the cellular uptake of cationic cell-penetrating peptides. Traffic. 2007; 8:848–66. [PubMed: 17587406]

[90]. Huh KM, Cho YW, Park K. PLGA-PEG Block Copolymers for Drug Formulations. Drug Development and Delivery. 2003; 3

[91]. Averineni RK, Shavi GV, Gurram AK, Deshpande PB, Arumugam K, Maliyakkal N, et al. PLGA 50:50 nanoparticles of paclitaxel: Development, in vitro anti-tumor activity in BT-549 cells and in vivo evaluation. B Mater Sci. 2012; 35:319–26.

[92]. Marrache S, Dhar S. Biodegradable synthetic high-density lipoprotein nanoparticles for atherosclerosis. P Natl Acad Sci USA. 2013; 110:9445–50.

[93]. Manoochehri S, Darvishi B, Kamalinia G, Amini M, Fallah M, Ostad SN, et al. Surface modification of PLGA nanoparticles via human serum albumin conjugation for controlled delivery of docetaxel. Daru. 2013; 21

[94]. Munro JC, Frank CW. Adsorption of lipid-functionalized poly(ethylene glycol) to gold surfaces as a cushion for polymer-supported lipid bilayers. Langmuir. 2004; 20:3339–49. [PubMed: 15875867]

[95]. Li D, Kaner RB. Shape and aggregation control of nanoparticles: Not shaken, not stirred. J Am Chem Soc. 2006; 128:968–75. [PubMed: 16417388]

[96]. Kumar G, Shafiq N, Malhotra S. Drug-loaded PLGA nanoparticles for oral administration: fundamental issues and challenges ahead. Crit Rev Ther Drug Carrier Syst. 2012; 29:149–82. [PubMed: 22475089]

[97]. Avgoustakis K. Pegylated poly(lactide) and poly(lactide-co-glycolide) nanoparticles: preparation, properties and possible applications in drug delivery. Current drug delivery. 2004; 1:321–33. [PubMed: 16305394]

[98]. Aggarwal P, Hall JB, McLeland CB, Dobrovolskaia MA, McNeil SE. Nanoparticle interaction with plasma proteins as it relates to particle biodistribution, biocompatibility and therapeutic efficacy. Advanced drug delivery reviews. 2009; 61:428–37. [PubMed: 19376175]

[99]. Hotze EM, Phenrat T, Lowry GV. Nanoparticle aggregation: challenges to understanding transport and reactivity in the environment. Journal of environmental quality. 2010; 39:1909–24. [PubMed: 21284288]

[100]. Lundqvist M, Stigler J, Elia G, Lynch I, Cedervall T, Dawson KA. Nanoparticle size and surface properties determine the protein corona with possible implications for biological impacts. Proc Natl Acad Sci U S A. 2008; 105:14265–70. [PubMed: 18809927]

[101]. Xiang CC, Yang F, Li M, Jaridi M, Wu NQ. Experimental and statistical analysis of surface charge, aggregation and adsorption behaviors of surface-functionalized titanium dioxide nanoparticles in aquatic system. J Nanopart Res. 2013; 15

[102]. Werth JH, Linsenbuhler M, Dammer SM, Farkas Z, Hinrichsen H, Wirth KE, et al. Agglomeration of charged nanopowders in suspensions. Powder Technol. 2003; 133:106–12.

[103]. Werth JH, Dammer SM, Farkas Z, Hinrichsen H, Wolf DE. Agglomeration in charged suspensions. Comput Phys Commun. 2002; 147:259–62.

[104]. Bagwe RP, Hilliard LR, Tan WH. Surface modification of silica nanoparticles to reduce aggregation and nonspecific binding. Langmuir. 2006; 22:4357–62. [PubMed: 16618187]

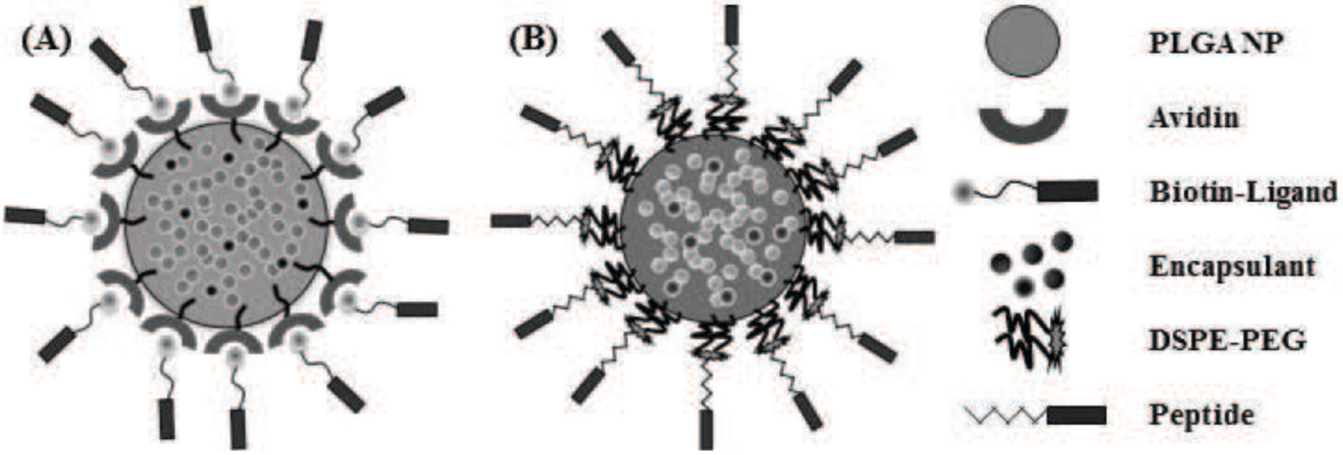

Figure 1.
Schematic of surface-modified NPs functionalized with either: (A) avidin-biotin-ligands (Av-ligand modified) or (B) DSPE-PEG-peptides (DSPE-modified).

A

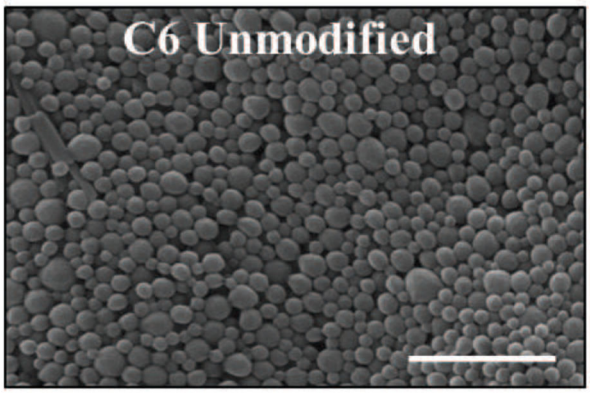

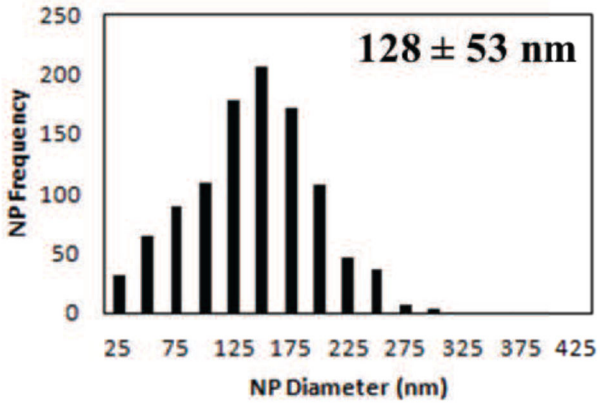

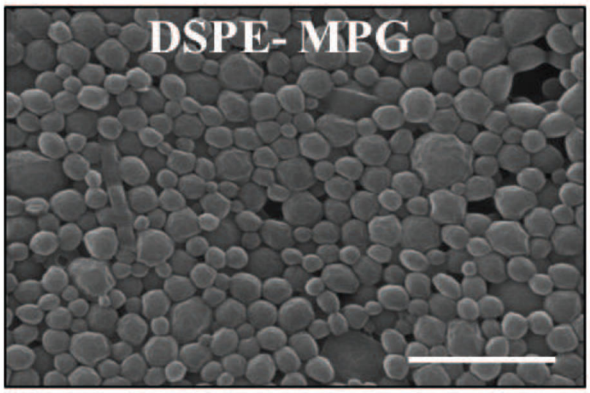

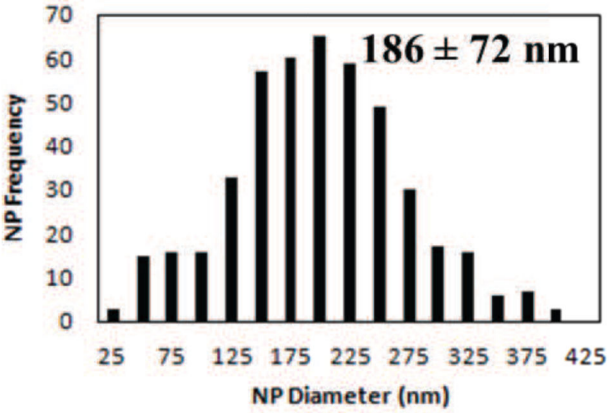

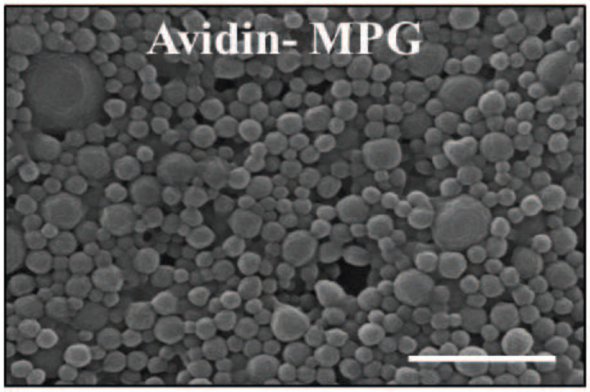

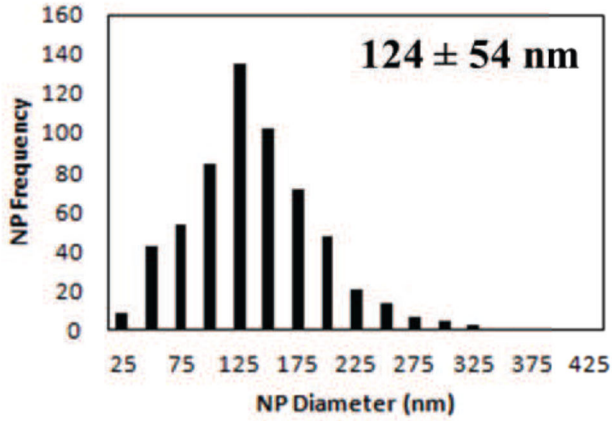

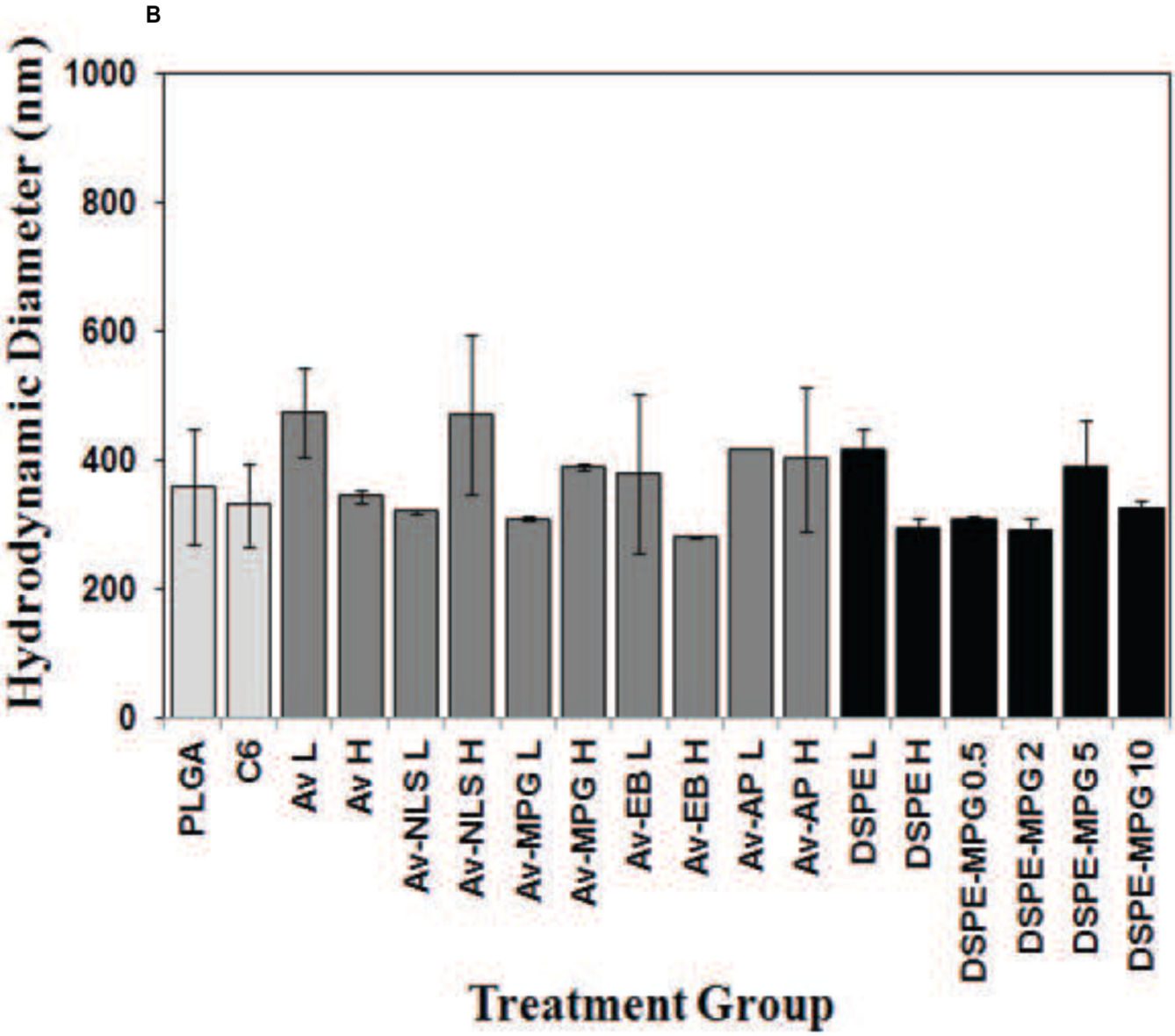

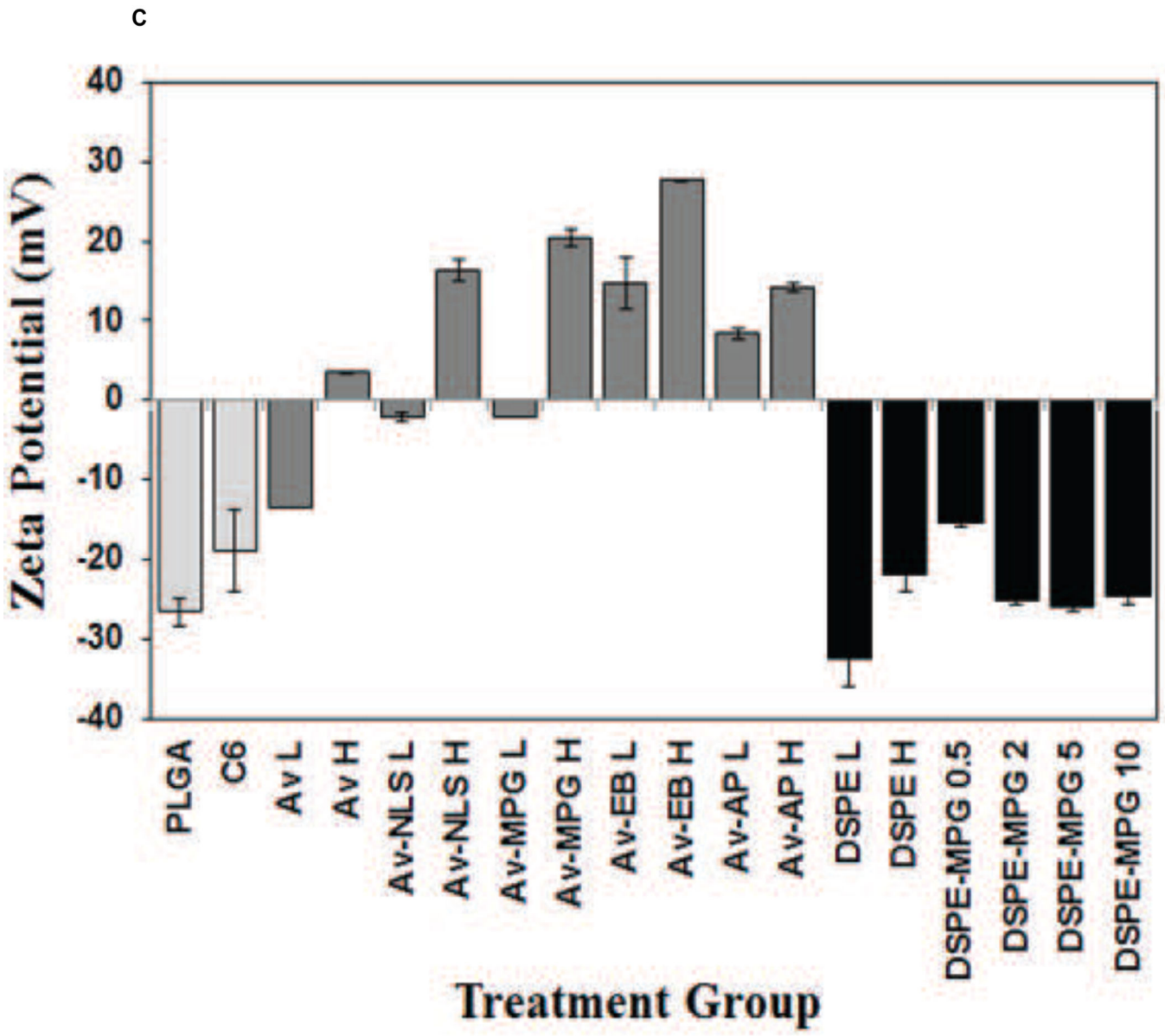

Figure 2.

(A) SEM of unmodified, DSPE-MPG and Av-MPG NPs, and the corresponding distribution of NP diameters for each formulation. Scale bar represents 1μm. (B) DLS values of NP hydrodynamic diameters. (C) Zeta potential values for all NPs.

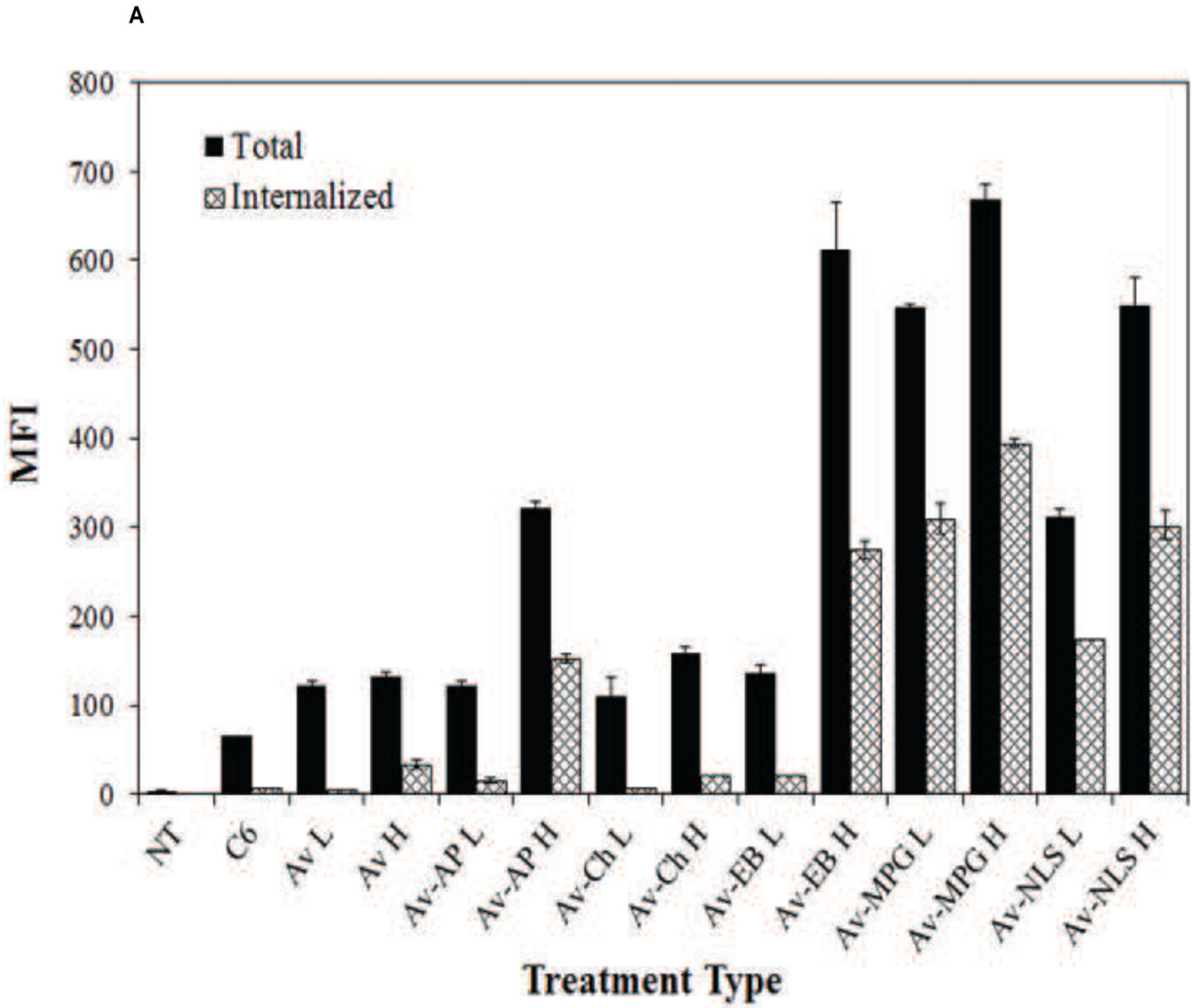

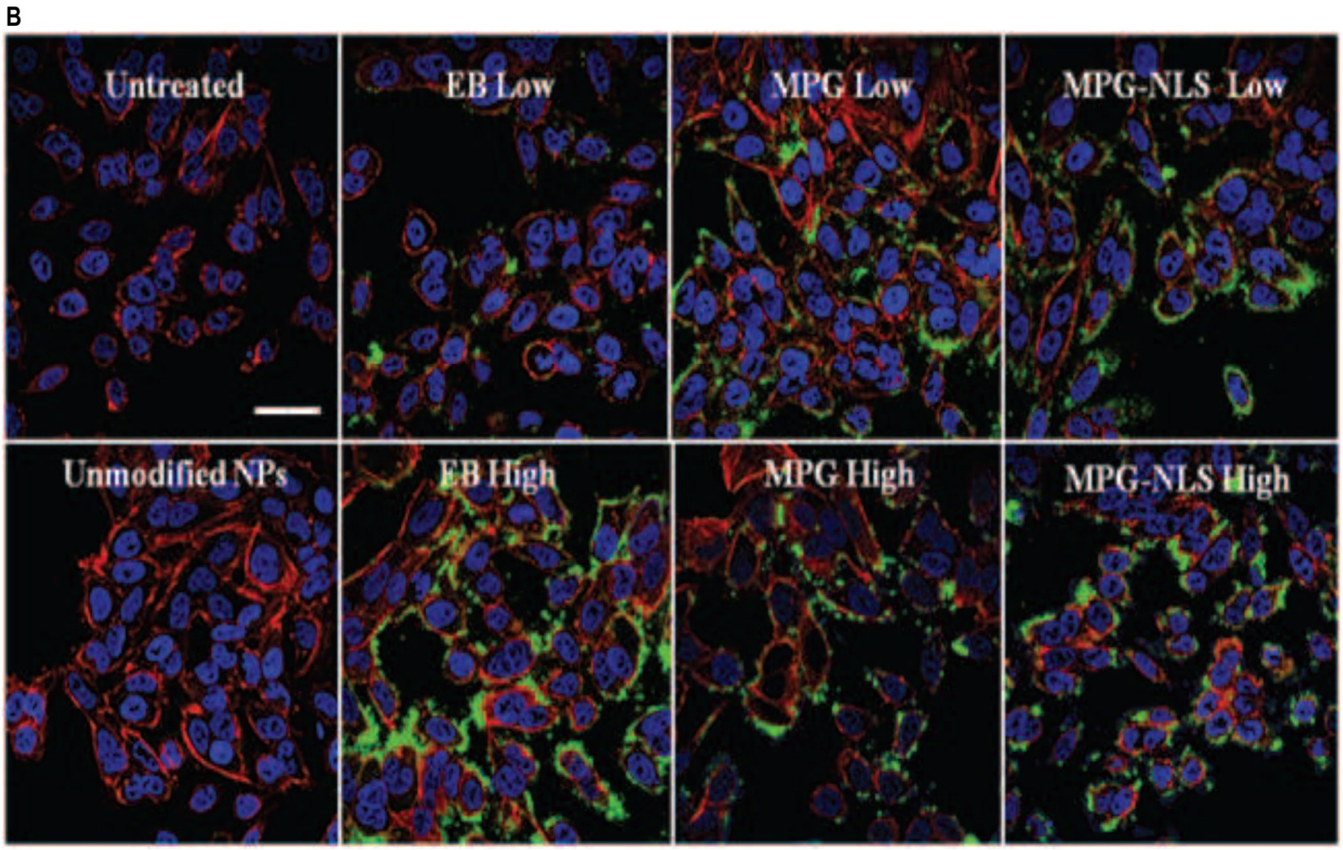

Figure 3.

(A) FACS analysis quantifying the effect of Av-ligand modification on NP total association (binding and internalization) and internalization in live HeLa cells after 2 hr. HeLa cells were exposed to 0.05 mg/mL of unmodified, low (L = 1 mg/mL), and high (H = 5 mg/mL) Av-ligand modified NPs for 2 hr. FACS data are presented as mean fluorescent intensity (MFI), and error bars represent standard deviation. (B) Confocal microscopy of live HeLa cells incubated with 200 μg/mL Av-ligand modified NPs for 2 hr. Cells were stained with Hoechst (blue) for the nucleus, Texas Red Phalloidin for actin (red), and incubated with Coumarin 6 (C6) NPs (green). White scale bar represents 50 μm.

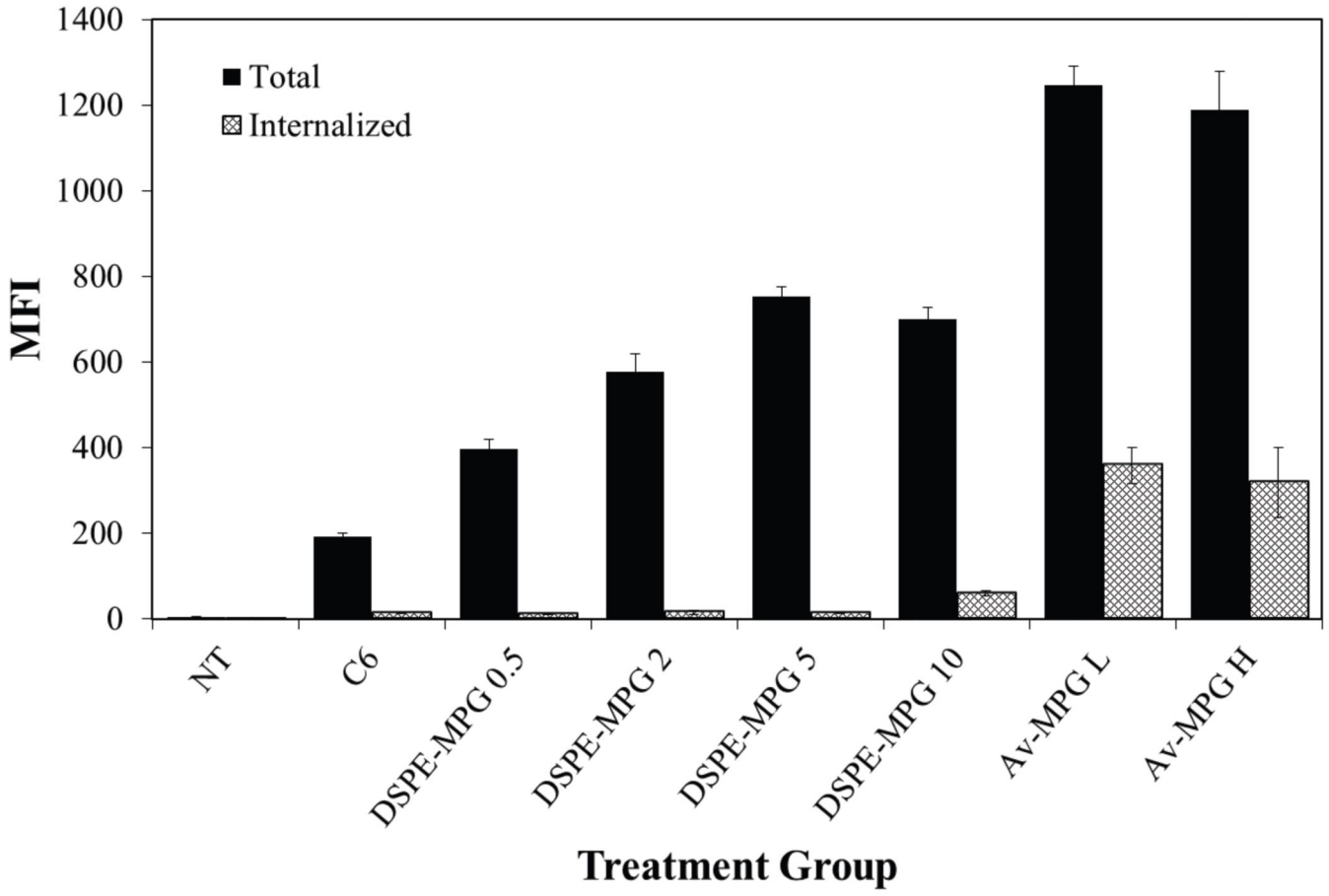

Figure 4.

Quantification of total cellular association and internalization of Av-MPG and DSPE-MPG NPs by FACS in live HeLa cells after 2 hr. HeLa cells were exposed to 0.05 mg/mL of DSPE-MPG (0.5, 2, 5, or 10 nmol/mg) or Av-MPG (L = 1mg/mL, H = 5 mg/mL) NPs for 2 hr. FACS data are presented as MFI, and error bars represent standard deviation.

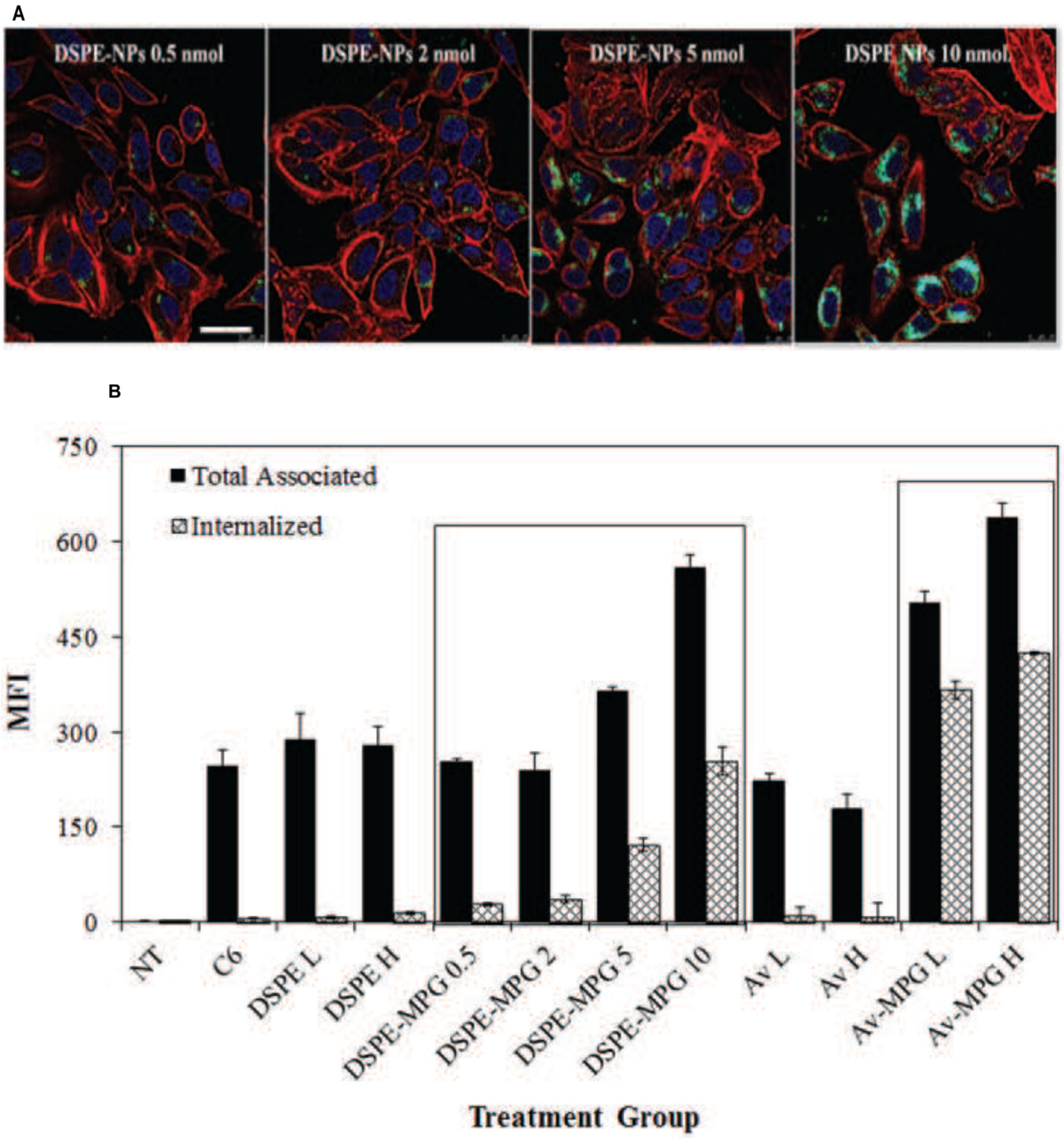

Figure 5.

(A) Confocal microscopy of HeLa cells incubated with 200 μg/mL DSPE-MPG (0.5, 2, 5, and 10 nmol/mg) modified NPs for 24 hr. Cells were stained with Hoechst (blue) for the nucleus, Texas Red Phalloidin for actin (red), and C6 NPs (green). Scale bar represents 25 μm. (B) Quantification and comparison of total cellular association and internalization of Av-MPG and DSPE-MPG NPs by FACS in live HeLa cells after 24 hr. HeLa cells were

exposed to 0.05 mg/mL of either Av or DSPE-modified NPs for 24 hr. Boxes around the DSPE-MPG and Av-MPG NP groups highlight the increase in binding and internalization as a function of surface modification density. FACS data are presented as MFI, and error bars represent standard deviation.

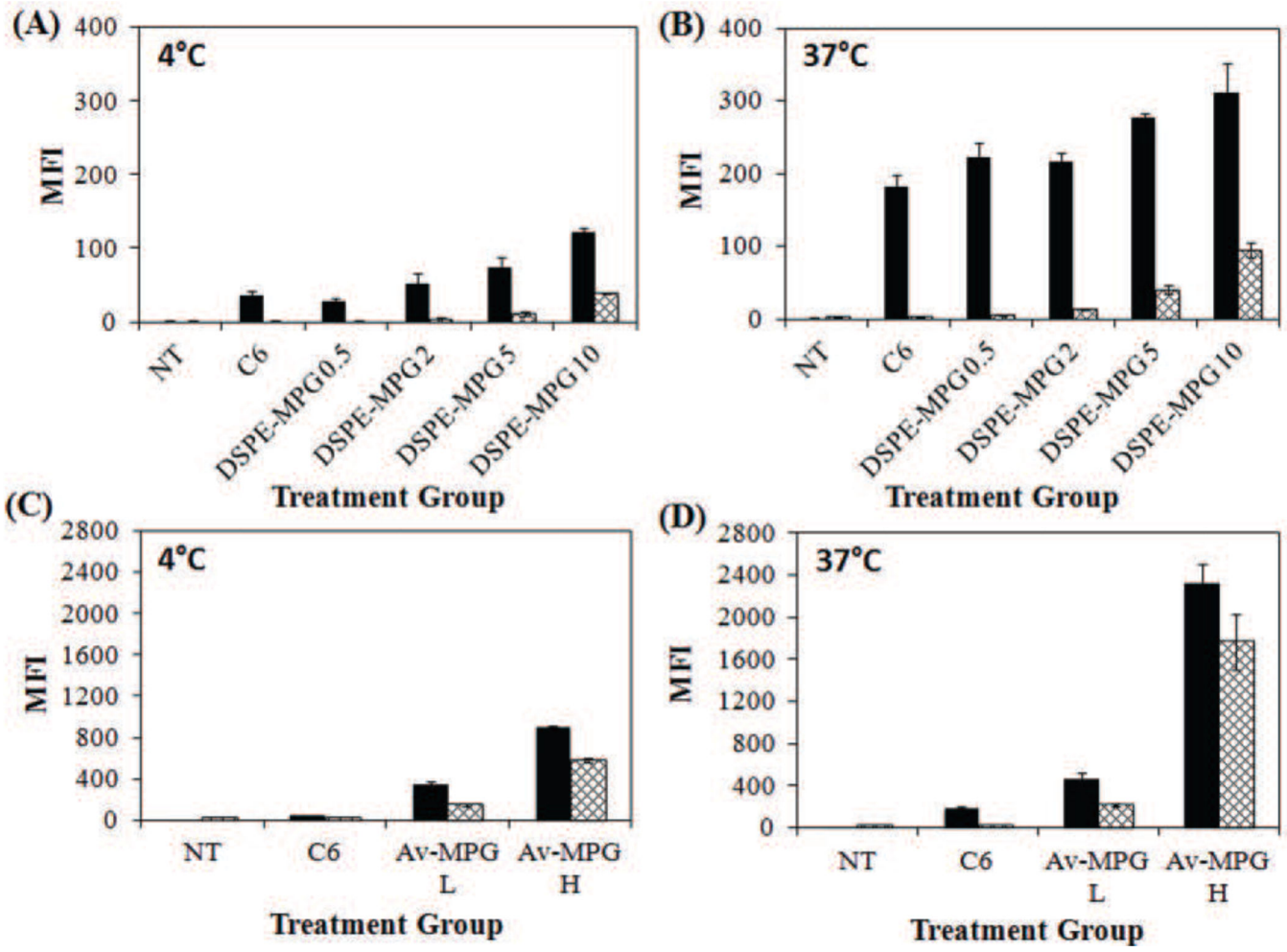

Figure 6.

Quantification of total cellular association and internalization by FACS in live HeLa cells. HeLa cells were incubated for 4 hr with 0.05 mg/mL of either DSPE-MPG (0.5, 2, 5, and 10 nmol/mg) NPs at: (A) 4 °C and (B) 37 °C, or Av-MPG (L = 1 mg/mL, H = 5 mg/mL) NPs at (C) 4 °C and (D) 37 °C. FACS data are presented as MFI, and error bars represent standard deviation.

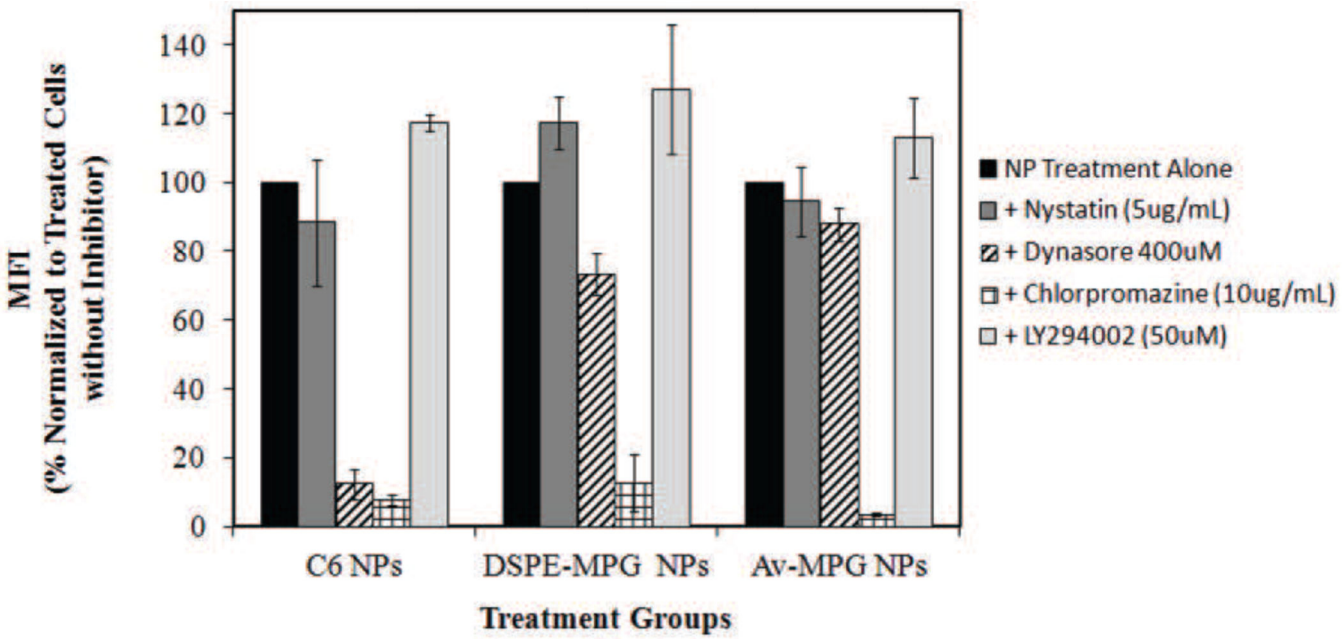

Figure 7.

Cellular uptake of unmodified, DSPE-MPG H (10 nmol/mg), and Av-MPG H (5 mg/mL) NPs in the presence of uptake inhibitors, as determined by FACS. Mean fluorescence intensity of cells incubated with NPs only (negative control) for each treatment group was set as 100%. Error bars represent standard deviation.

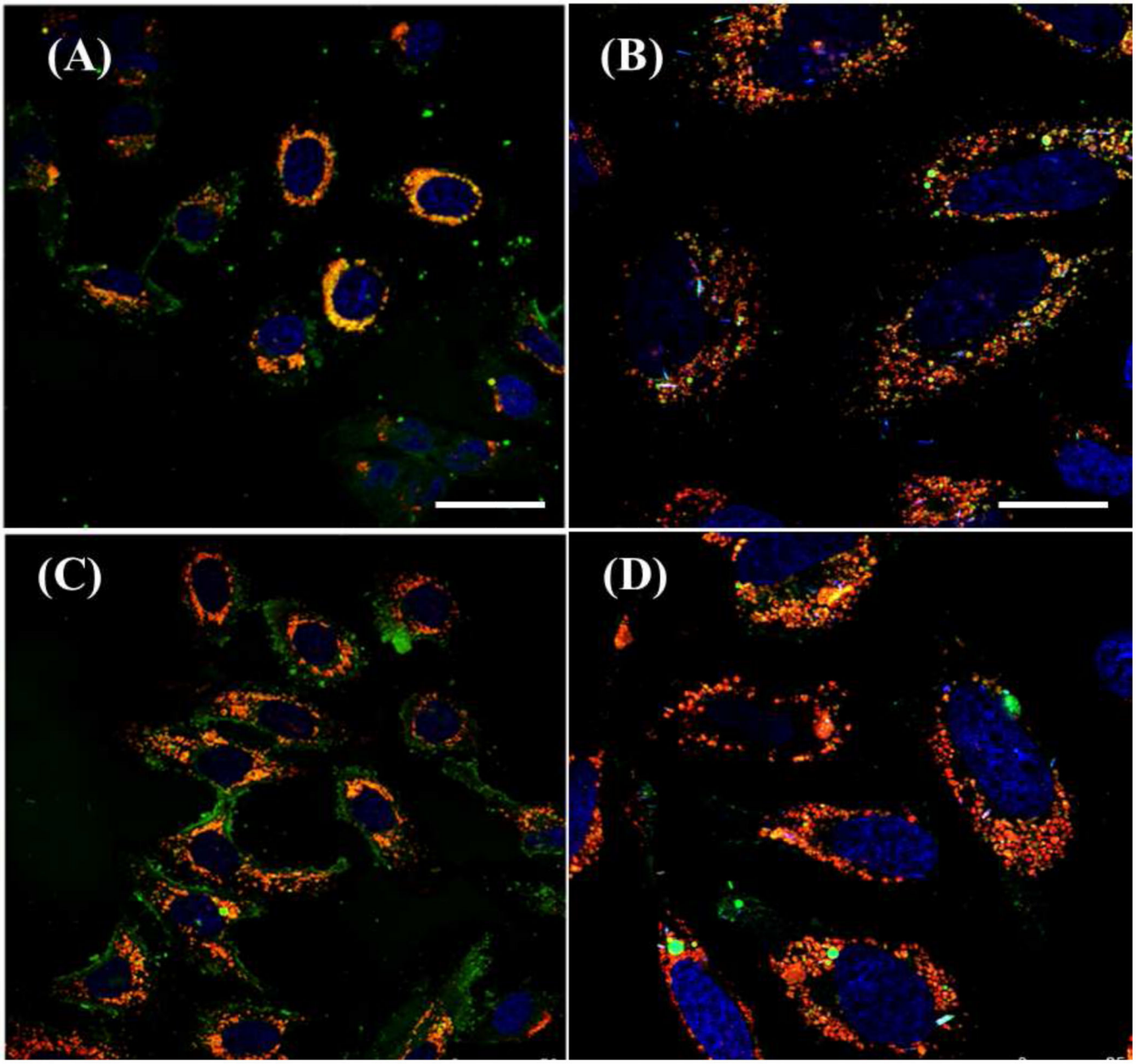

Figure 8.

Confocal microscopy of lysosome-NP colocalization in live HeLa cells. HeLa cells were incubated with 200 μg/mL (A, B) DSPE-MPG H (10 nmol/mg), or (C, D) Av-MPG H (5 mg/mL) NPs for 24 hr. Figures B and D show magnification of similar regions as A and C, respectively. Cells were stained with Hoechst (blue) for the nucleus, LysoTracker® Red (red) for lysosomes, and C6 NPs (green). Panels (A,C) show cells at 20× magnification and (B,D) show cells at 40× magnification. Scale bars represent 50 and 25 μm respectively, for the left and right panels.

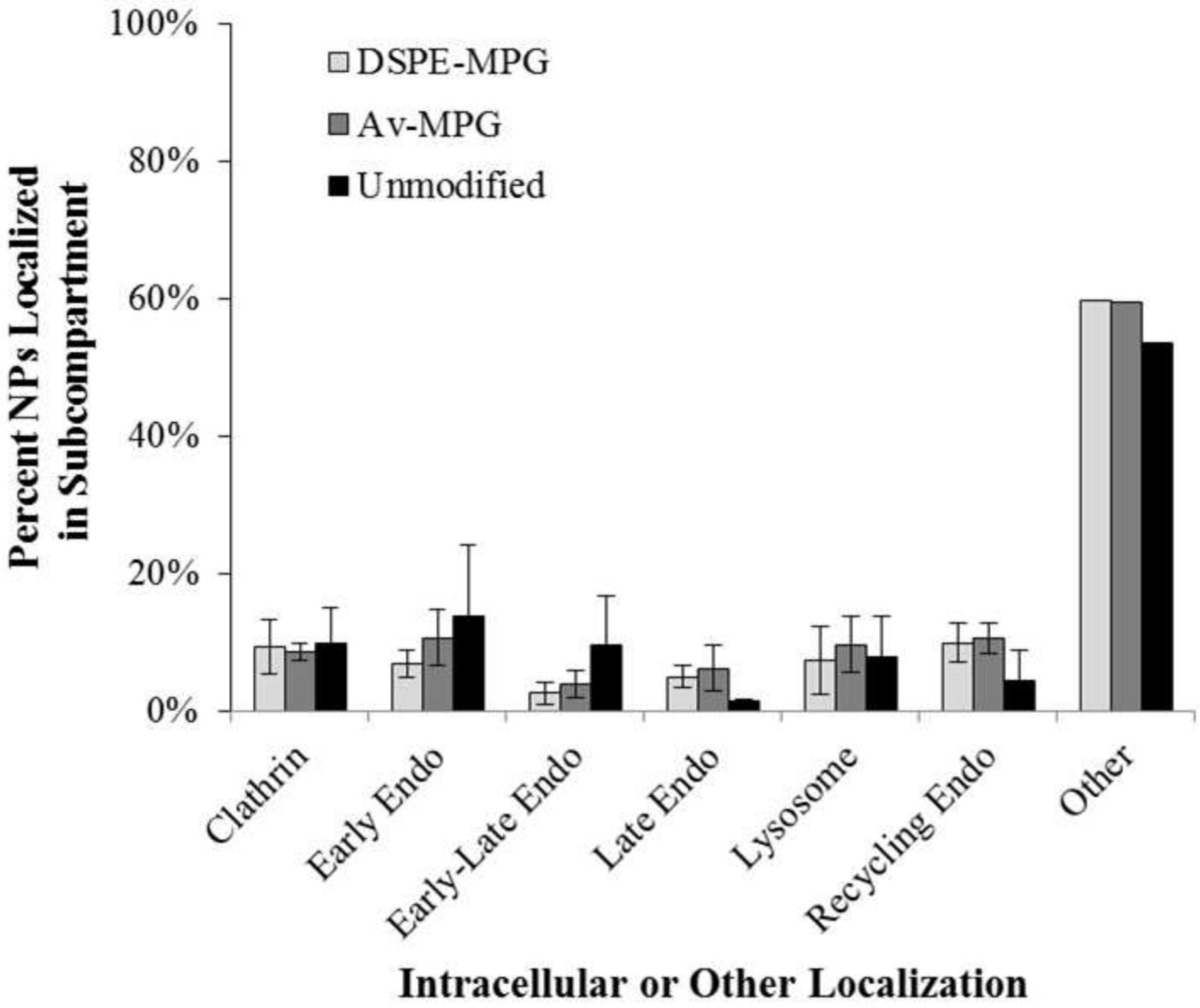

Figure 9.

Colocalization of DSPE-MPG, Av-MPG, and unmodified NPs with intracellular protein markers after 24 hr. Percent of NPs colocalized in subcompartments, relative to total NPs. Error bars represent standard deviation.

Table 1

Theoretical versus actual surface coverage density of Av-MPG and DSPE-MPG NPs.

Sample	Theoretical Coverage (nmol/mg)	Actual (nmol/mg)	% Incorporation	# Molecules/NP
Av-MPG L	0.14	0.12	84%	158
Av-MPG H	0.72	0.72	100%	944
DSPE-MPG 0.5	0.5	0.45	90%	585
DSPE-MPG 2	2	1.79	90%	2321
DSPE-MPG 5	5	2.71	54%	3514
DSPE-MPG 10	10	4.09	41%	5308